Nitrogen gas–solid reaction process and basic magnetism of the interstitially modified rare-earth 3*d* transition-metal nitrides $R_2Fe_{17}N_3$ (R=Y, Ce, Nd, Sm) and $Y_2Co_{17}N_3$

Keiichi Koyama
Institute for Materials Research, Tohoku University, Sendai 980 8577, Japan

Hironobu Fujii*
Faculty of Integrated Arts and Sciences, Hiroshima University, 1-7-1 Higashi-Hiroshima 739 8521, Japan
(Received 15 June 1999; revised manuscript received 12 November 1999)

In this paper, we present our recent results of studies of the nitrogen absorption process, magnetization measurements, and neutron powder-diffraction measurements for interstitially modified nitrides $R_2Fe_{17}N_3$ (R = Y, Ce, Nd, and Sm) and $Y_2Co_{17}N_3$. (1) The studies of nitrogen absorption rates in the Sm_2Fe_{17} under various N_2-gas pressure up to 6 MPa indicated that the nitrogen absorption into grain interior is promoted by diffusion of nitrogen atoms under low N_2-gas pressure, while under high N_2-gas pressure, the nitrogen absorption is promoted by the grain growth of fully nitrogenated phase $Sm_2Fe_{17}N_3$ rather than the diffusion, making high-pressure nitrogenation effective for synthesizing high-quality nitrides. (2) The high-field magnetization measurements of the Nd_2Fe_{17} and $Nd_2Fe_{17}N_3$ single crystals at 4.2 K indicated that interstitial modification of nitrogen atoms gives rise to a strong enhancement of crystalline electric field (CEF) acting on R atoms, leading to almost three times larger CEF-parameter A_2^0 upon nitrogenation. (3) Neutron powder-diffraction studies of Y_2Fe_{17} and $Y_2Fe_{17}N_{3.1}$ with rhombohedral structure indicated that the N atoms fully occupy at the 9*e* site. The introduction of N atoms into Y_2Fe_{17} brought such a strong modification in the Fe magnetic moment that the moment of the 18*f*-Fe atoms being the nearest to the 9*e*-N atoms is the smallest, whereas the 6*c*-Fe and/or 18*h*-Fe atoms being relatively farther from the 9*e*-N atoms have the largest moments at 10 K. The results obtained are discussed on the basis of the calculated electronic band structures.

I. INTRODUCTION

One of the methods for fabricating new magnetic materials is to introduce nonmetallic atoms such as H, B, C, or N with small atomic radius into host metals, alloys, and compounds. In such modified compounds, some hydrides have been synthesized by the solid-gas reaction since the 1960s and their magnetic properties have been clarified.[1] However, no significant improvement in the intrinsic magnetic properties was observed upon hydrogenation. For instance, introduction of hydrogen into interstitial sites in R_2Fe_{17} have brought an increase in the Curie temperature T_C as well as the saturation magnetization M_s without changing the crystal symmetry, but have not led to any significant improvement in the uniaxial magnetic anisotropy.[2] On the contrary, the introduction of hydrogen into some Co and Ni intermetallics brought rather decrease in T_C as well as M_s.

Introduction of B or C into them have been examined by melting methods in order to expand interatomic distances between 3*d*-transition atoms, especially Fe atoms, in the 1980s. In those efforts, a type of permanent magnetic material $Nd_2Fe_{14}B$ has been discovered by Sagawa *et al.*,[3] and Croat *et al.*[4] The details of the basic magnetism have been reviewed by Herbst.[5] The magnetic characteristics of $Nd_2Fe_{14}B$ with a tetragonal structure are $M_s = 1.60$ T, $\mu_0 H_a = 7$ T at room temperature and $T_C = 588$ K. The achieved energy product have reached over 360 kJ/m,[3] which significantly exceeded those of all the other type of magnets. In the melting process, a small amount of C can only occupy some interstitial sites in some 2:17- or 1:12-type intermetallics.[6] As a result of incomplete occupation, improvement of magnetism by introduction of C have not been satisfactorily established.

On the other hand, introduction of N into intermetallics has been examined by applying the gas–solid reaction in late 1980s.[7] Finally, the interstitially modified compound $Sm_2Fe_{17}N_3$ was discovered by Coey and Sun in 1990.[8] The nitride was prepared by heating Sm_2Fe_{17} at 773 K under a nitrogen gas or an ammonia atmosphere. Then, the crystal lattice expands more than 6% to accommodate three nitrogen atoms at the interstitial sites. The Curie temperature T_C increases dramatically from 398 to 752 K. The saturation magnetization of $Sm_2Fe_{17}N_3$ ($M_s = 1.54$ T) is comparable to that of $Nd_2Fe_{14}B$ and the uniaxial magnetic anisotropy ($\mu_0 H_a = 21$ T) is three times as strong as that in $Nd_2Fe_{14}B$ at room temperature.[9] Since the discovery of the 2:17-type nitrides, worldwide efforts have been devoted not only to the clarification of the mechanism of improvement of basic magnetism, but also to the development of the promising interstitial compound $Sm_2Fe_{17}N_3$ into high performance permanent magnets.[6] However, the details of the fundamental magnetic properties are not well understood at present stage. The reason is that the quality of the host and nitride samples was not so good and the data accumulated were widely scattered. Especially, only little data on the change of the Fe moment at each site in the Fe sublattice, and information on the origin of the strong anisotropy enhancement upon nitrogen uptake has been accumulated so far. Therefore, much attention has been paid to the study of the gas-phase interstitial modification process itself because of obtaining high-quality nitrides.

So far, gas-phase nitrogenation reactions have been mainly conducted at 673–773 K on finely ground powder under moderate N_2-gas pressures less than 1 MPa,[8] nitrogen containing gas NH_3 (Ref. 8) or mixed gas such as NH_3+H_2 (Ref. 10) or N_2+H_2.[11] All these nitrogenation processes, more or less, give rise to a small but noticeable segregation of α-Fe phase in the powder samples during nitrogenation. Furthermore, Isnard *et al.* employed a high-pressure nitrogenation technique up to 15 MPa for studying neutron-diffraction experiments on $R_2Fe_{17}N_3$.[12] They pointed out that the technique enabled us to synthesize high-quality nitrides and to attain the maximized magnetic properties. In our group, independently, high-pressure N_2 gas nitrogenation process was also developed as a suitable one for synthesizing some high-quality 2:17 nitrides.[13,14] This process offered the following two advantages: one is to suppress the segregation of the α-Fe phase on the powder during nitriding, and the second is to reach a full nitrogenation of $N\sim 3$ within a relatively short time of treatment. The details of nitrogen absorption process are described in this paper.

From the technological aspects, on the other hand, various techniques have been applied to $Sm_2Fe_{17}N_3$ for producing both isotropic and anisotropic magnets.[6] Unfortunately, $Sm_2Fe_{17}N_3$ is metastable and disproportionate at temperatures higher than 600 °C. Thus the conventional high-temperature powder metallurgy was not applicable to product permanent magnets. The problem is to either improve the stability or develop a suitable processing route for making bulk permanent magnets. Recently, Machida *et al.*[15] have reported that the powders of $Sm_2Fe_{17}N_3$ prepared by ball milling in hexane solution containing a surface-active agent provided high-performance characteristics; the remanence $B_r = 1.2-1.3$ T, the coercivity $\mu_0 H_c = 1.1-1.4$ T and the resultant energy product $(BH)_{max}=320\ kJ/m^3$. More recently, Kawamoto *et al.*[16] of the Sumitomo Metal Mining Corporation have reported that $Sm_2Fe_{17}N_3$ prepared by the reduction-diffusion method are in mass production as a bonded magnet powder, which reaches as high as $(BH)_{max}=320\ kJ/m^3$. Furthermore, Sasaki *et al.*[17] have obtained higher-performance characteristics in $Sm_2Fe_{17}N_3$ with $B_r=1.4$ T, $\mu_0 H_c = 1.23$ T, and $(BH)_{max}=330\ kJ/m^3$ by the similar ball milling method as Machida *et al.* used without exposing the sample in air.

In this paper, we will present our results of the following fundamental and complementary experiments; (1) clarification of nitrogen absorption process in Sm_2Fe_{17} under N_2-gas high-pressure atmospheres up to 6 MPa, which is performed for synthesizing high-quality nitrides,[14] (2) magnetic measurements of high-quality $R_2Fe_{17}N_3$ powder samples where $R=$Y, Ce or Sm and $Y_2Co_{17}N_3$, which is carried out for clarifying some changes in the macroscopic magnetism upon nitrogenation,[18,19] (3) the high-field magnetization measurements of single crystals of Nd_2Fe_{17} and $Nd_2Fe_{17}N_3$,[20,21] which is done for clarifying the modification mechanism of the crystalline electric field (CEF) due to the introduction of nitrogen atoms in the 2:17 systems, and (4) neutron powder-diffraction studies of $Y_2Fe_{17}N_3$, which is done for clarifying the detail of interstitial occupations of nitrogen and the modification mechanism of the Fe moments on nonequivalent sites in the Fe sublattice.[22]

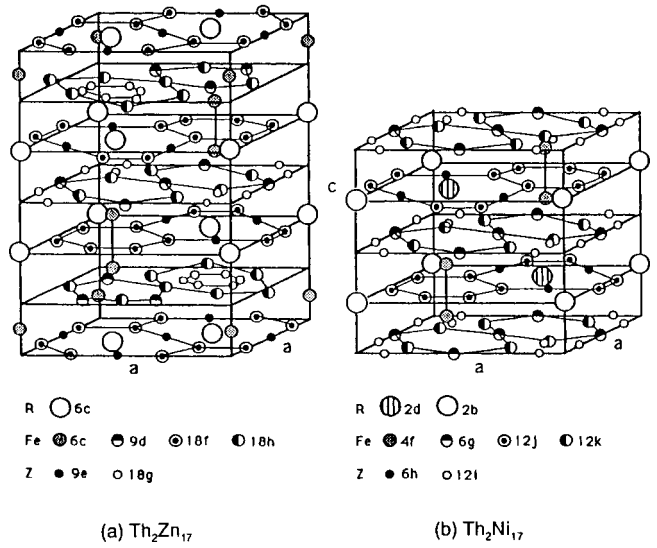

FIG. 1. Crystal structures of R_2Fe_{17}: (a) rhombohedral Th_2Zn_{17} type (left) and (b) hexagonal Th_2Ni_{17} type (right) structures. Here, R represents the rare-earth sites, Fe represents the iron sites, and Z represents the interstitial sites.

II. CRYSTAL STRUCTURE

Before proceeding, we will describe crystal structures of R_2Fe_{17} and their nitrides. As is shown in Fig. 1, the R_2Fe_{17} intermetallics crystallize in the rhombohedral Th_2Zn_{17}-type structure for light rare earths or the hexagonal Th_2Ni_{17}-type one for heavy rare earths and Y. Among them, the compounds with $R=$Ce, Gd, Tb, and Y crystallize in either the rhombohedral or hexagonal structure, depending on heat-treatment temperature.[23] The difference in stability between the two types of structures is probably so small that the transition from one to the other can proceed by displacement of metal atoms without any diffusionlike martensitic transformation.[24,25] Therefore, it is not so easy to obtain the two types of each single phase independently.

Both the rhombohedral Th_2Zn_{17}-type and hexagonal Th_2Ni_{17}-type structures are derived from an ordered substitution of a pair of Fe atoms (dumbbell) for each third rare-earth atom in the basal plane in a hexagonal $CaCu_5$-type structure;

$$3(RFe_5)-R+2Fe(\text{dumbbell})\rightarrow R_2Fe_{17}. \qquad (1)$$

If the substituted sublayers are stacked in the sequence ABCABC$---$ along the c axis for a $CaCu_5$-type structure, the rhombohedral Th_2Zn_{17}-type structure is formed. On the other hand, if the stacking sequence is, instead, ABAB$---$ along the c axis, then the hexagonal Th_2Ni_{17}-type structure is formed. However, a partial disorder has been observed in the actual structure of the hexagonal R_2Fe_{17} with $R=$Lu, Ho, and Y,[26–28] which is induced by some exchange of some R atoms at the $2b$ site for the Fe-dumbbell atoms and vice versa. Furthermore, the hexagonal 2:17 system has two crystallographically nonequivalent rare-earth sites ($2b$ and $2d$ sites), while the rhombohedral 2:17 system has only one crystallographic rare-earth site ($6c$ site). Therefore, magnetic structures of the rhombohedral 2:17 system are much more suitable to understand basic magnetism than the hexagonal

2:17 system. From the above reason, we have studied basic magnetism for only the rhombohedral R_2Fe_{17} systems and their nitrides in this work.

In the rhombohedral 2:17 nitrides, it has been clarified that the nitrogen atoms preferentially occupy the 9*e* sites by neutron-diffraction experiments of $R_2Fe_{17}N_\delta$ with $R=$Ce,[12] Pr,[29] Nd,[12,30–36] or Th (Ref. 37) as shown in Fig. 1. However, we notice that the occupation of nitrogen is not completely full in their data and the occupation factor *n* scatters from 0.60 to 0.99 by the authors.

III. EXPERIMENTAL PROCEDURES

The host compounds were prepared by arc melting the constituent elements of 99.9% purity under an argon gas atmosphere for all the systems except for the Sm system, and by induction melting of the starting elements for the Sm system. After annealing them at 1373–1393 K for one-two weeks, all the samples were confirmed to be a single phase with the Th_2Zn_{17}-type rhombohedral structure. Before nitrogenation, the ingots were pulverized into powder in a glove box with an argon atmosphere. Then, nitrogenation was performed for all the systems by the high-pressure N_2-gas method. That is; the samples were nitrogenated by heating at 713–733 K for 60–90 h under N_2-gas pressures up to 6 MPa. All the nitrides obtained were almost a single phase with the same structure as the host compounds. The nitrogen concentration was estimated from the increase in mass upon nitrogenation. Furthermore, the single crystal of Nd_2Fe_{17} was prepared in a Ta crucible by a flux method using excess Nd as a flux[38] and the nitrogenation was performed by almost the same high-pressure N_2-gas method as used for the other systems after making some cracks into it by hydrogenation. The details of preparation of the single-crystal nitride will be described in Sec. VI.

Morphological and microscopic composition analyses were performed using a scanning electron microscope (SEM) and an electron-probe microanalyzer (EPMA), from which we could detect the spatial nitrogen atom distribution in the powder. To check the phases contaminated in the samples during nitrogenation, x-ray diffraction studies were performed at room temperature using Cu $K\alpha$ radiation. Magnetization was measured using a vibrating-sample magnetometer up to 1.6 T in the temperature range from 4.2 to 900 K. Measurement of high-field magnetization up to 27 T was performed for single-crystalline Nd_2Fe_{17} host compound and the nitride, and for the powder of $Sm_2Fe_{17}N_3$ using a hybrid magnet set up at High-Field Laboratory, Tohoku University. Neutron powder-diffraction studies were carried out for the rhombohedral Y_2Fe_{17} and the nitride at 10 K using a high-resolution neutron diffractometer installed in JRR-3M of Japan Atomic Energy Research Institute at Tokai.

IV. NITROGEN-ABSORPTION PROCESS UNDER HIGH-PRESSURE N_2 GAS

Until now, the studies of nitrogenation process have been conducted by many different researchers using different experimental techniques, such as Kerr microscopic observations, x-ray-diffraction studies, *in situ* neutron powder diffraction studies, thermogravimetric analysis, micrograph studies applying metallography and electron-probe microanalyzer (EPMA) techniques and so on.[33,39–47,96,97] However, it has been still an open question whether the metastable nitride is a simple gas-solid solution with a continuous range of intermediate nitrogen contents,[40,42] or it is a two-phase mixture of nitrogen-poor and nitrogen-rich phases.[34,43–47,96,97]

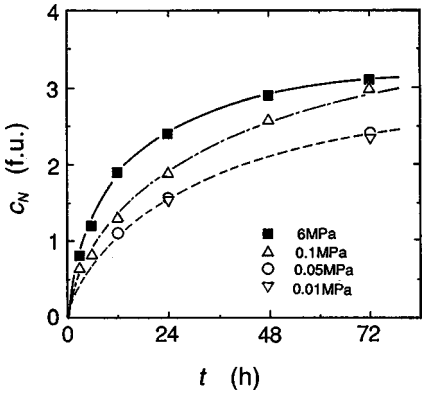

FIG. 2. Nitrogen concentration in the Sm_2Fe_{17} powder sample as a function of the reacting time at 733 K under various N_2-gas pressures. The particle size of the powder is about 42 μm.

At first, for clarifying the nitrogen absorption process in the 2:17 system under high N_2-gas pressures, we studied the time evolution of the nitrogen absorption rate and nitrogen atom distribution in the Sm_2Fe_{17} powder as a function of N_2-gas pressure at various temperatures.[14] The average size of the powder sample used in this experiment is $\sim 42 \pm 10$ μm in diameter, which are composed of an assembly of single-crystal particles.

In Fig. 2, the nitrogen concentration is shown as a function of the reacting time at 733 K under various N_2-gas pressures. We notice the following characteristic features: (1) it takes the reacting time more than 72 h to fully nitrogenate Sm_2Fe_{17} with ~ 42 μm in diameter even under 6 MPa of N_2 gas pressure at 733 K, (2) the nitrogen absorption rate gradually decreases with decreasing the N_2-gas pressure P_{N2}, and (3) the absorption rate is independent of pressure under P_{N2} less than 0.05 MPa, suggesting that the rate-determining step in lower N_2 gas pressures is the diffusion process of nitrogen atoms in the Sm_2Fe_{17} grains. To clarify whether the Sm_2Fe_{17} nitride with intermediate nitrogen concentration is a simple gas–solid solution phase or a two-phase mixture of nitrogen-free Sm_2Fe_{17} and fully nitrided $Sm_2Fe_{17}N_3$ phases, we compared the x-ray-diffraction patterns at an intermediate stage under various pressures with each other. The results obtained are shown in Fig. 3. We notice that the peak separation for the (113), (300), or (204) reflections between Sm_2Fe_{17} and $Sm_2Fe_{17}N_3$ is clear in the nitride with a nitrogen content of $x=1.9$ for the sample prepared by reacting them at 733 K under N_2 gas pressure of 6 MPa, while the separation becomes unclear for the sample prepared under the lower pressures below 0.05 MPa. Therefore, a simple solid solution with continuous range of intermediate nitrogen content may be stabilized under lower pressures below 0.05 MPa because the critical temperature could be below 733 K.

In the above case, a question is why the two-phase mixture appears in the nitride prepared under $P_{N2}=6$ MPa. To answer it, we performed microscopic composition analysis of the nitrogen atoms in the $Sm_2Fe_{17}N_x$ powder sample using

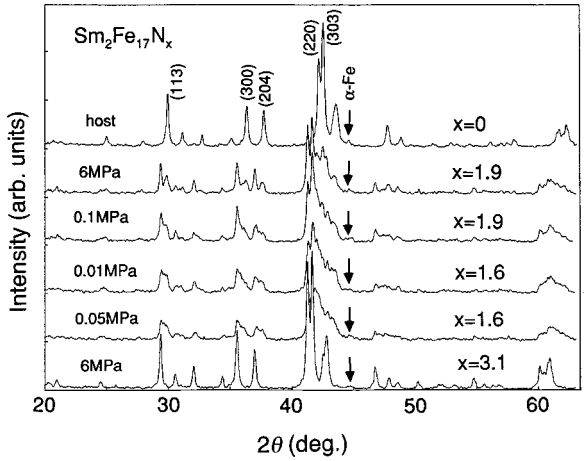

FIG. 3. X-ray-diffraction patterns of the Sm_2Fe_{17} powder with $x=1.6$ to 1.9 at an intermediate stage in nitrogenation under various N_2-gas pressures. The x-ray patterns for the host and fully nitrogenated samples are also included in this figure.

the EPMA equipment. Here, it should be noted that the beam width of EPMA probe is several micrometers. Figures 4 and 5 show, respectively, the EPMA line profiles and the corresponding SEM image figures on cross section for the $Sm_2Fe_{17}N_x$ powder with intermediate N-atom contents, which was obtained by reacting at 733 K for 12 h under 0.1 and 6 MPa. We can see some differences in N-atom distributions between 0.1 and 6 MPa. For the nitrogenated powder at 733 K for 12 h under 0.1 MPa, the N atoms penetrate into the interior from the surface of the powder and the N-content gradually decreases with increasing the depth from surface into interior. On the other hand, for the $Sm_2Fe_{17}N_x$ powder prepared under 6 MPa, the N-content remains constant (fully nitrogenation) with increasing the depth from surface until reaching a critical depth, beyond which the content rapidly decreases with increasing the depth, compared with the former profile. Systematically, we recorded the EPMA line profiles of the N atom distribution in $Sm_2Fe_{17}N_x$ prepared by changing the reacting time from 6 to 48 h at 733 K under 0.1 and 6 MPa. The results obtained are summarized in Fig. 6. Here, the nitrogen concentration c_N on the surface of powder is normalized at $c_N=3.0$ for all the powder. We can recognize some characteristic features from Fig. 6: (1) the arrival

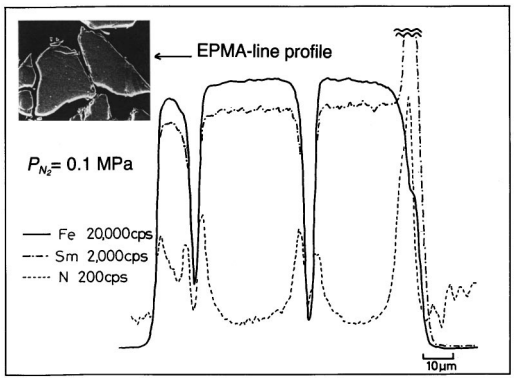

FIG. 4. EPMA line profiles of Fe, Sm, and N elements in the $Sm_2Fe_{17}N_x$ powder obtained by reacting at 733 K for 12 h under 0.1 MPa. The inset shows the corresponding SEM figure.

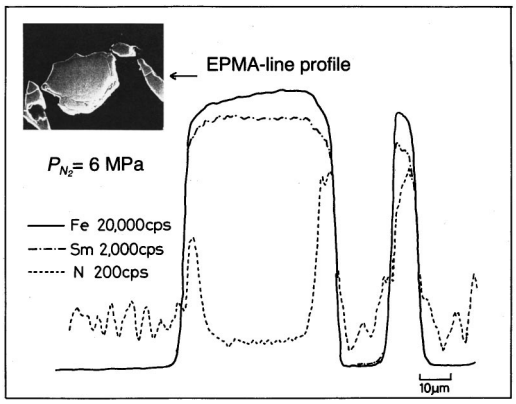

FIG. 5. EPMA line profiles of Fe, Sm, and N elements in the $Sm_2Fe_{17}N_x$ powder obtained by reacting at 733 K for 12 h under 6 MPa. The inset shows the corresponding SEM figure.

depth of the N atoms from surface of the powder is independent of the nitriding pressure P_{N2}, for example, it reaches ~ 15 μm from the surface by heating at 733 K for 12 h in both 0.1 and 6 MPa, (2) the fully nitrogenated depth at $P_{N2}=6$ MPa is almost twice as thick as $P_{N2}=0.1$ MPa, indicating that the grain growth of fully nitrogenated phase is dominant under high N_2-gas pressure.

On the basis of the N atomic distribution in $Sm_2Fe_{17}N_x$, we discuss the nitrogen absorption process under various N_2-gas pressures. In the nitrogen gas–solid reaction in powder samples, there are three fundamental reaction processes: (1) the nitrogen dissociation process from the N_2-gas phase into N atoms ($N_2 \rightarrow 2N$) on the surface of a powder, (2) the nitrogen atom diffusion process into the interior of powder from the surface ($Sm_2Fe_{17}+1/2N_2 \rightarrow Sm_2Fe_{17}N_x$) ($x<3.0$) and (3) grain growth of the fully nitrogenated phase

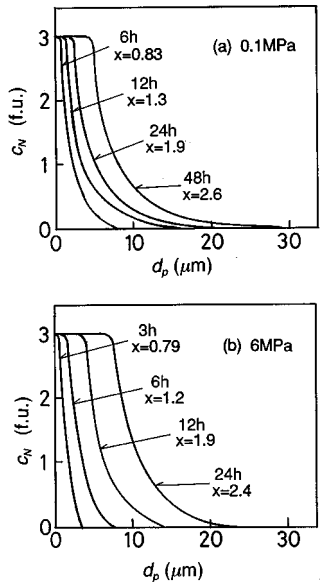

FIG. 6. Nitrogen atom distribution as a function of the depth from the surface of powder for various reacting times in nitrogenation at 733 K (deduced from the recording of the corresponding EPMA line profiles of N element) under (a) 0.1 MPa and (b) 6 MPa. Here, x is average nitrogen contents in powder. The nitrogen concentration c_N on the surface of powder is normalized at $c_N=3.0$ for all the samples.

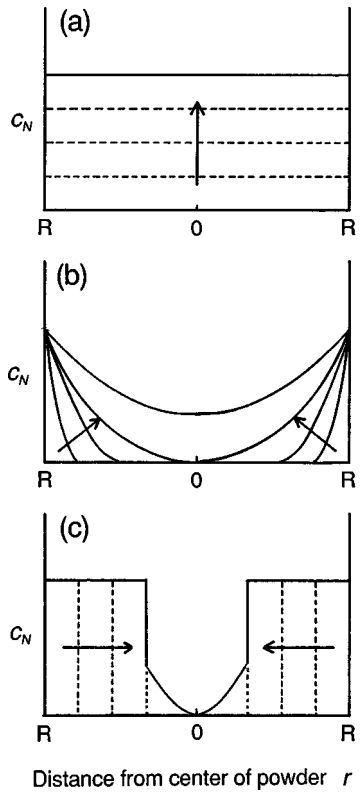

FIG. 7. Nitrogen distribution profiles for three fundamental reaction processes: (a) nitrogen dissociation process; (b) nitrogen diffusion process; (c) grain growth process of the fully nitrided phase.

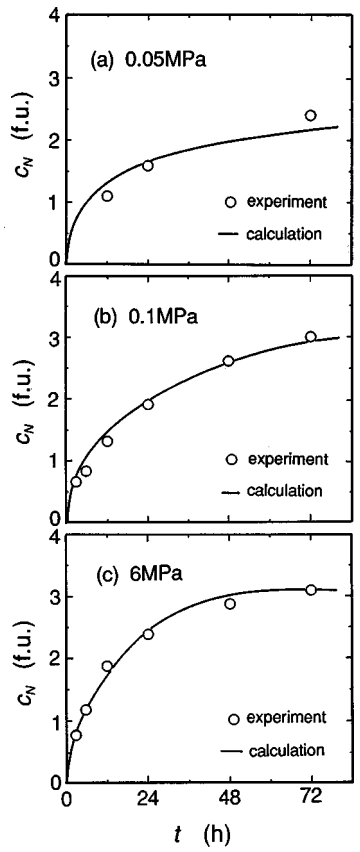

FIG. 8. Nitrogen concentration $c_N(t)$ as a function of nitrogenation time t at 733 K under (a) 0.05 MPa (b) 0.1 MPa and (c) 6 MPa. The solid lines are the calculated curves using the diffusion constant $D=3.1\times10^{-16}\,m^2\,s^{-1}$ at 733 K and the velocity of grain growth of the fully nitrided phase (a) $V_G=0$ for 0.05 MPa, (b) $V_G=4.5\times10^{-11}\,m\,s^{-1}$ for 0.1 MPa and (c) $V_G=9.0\times10^{-11}\,m\,s^{-1}$ for 6 MPa at 733 K.

$Sm_2Fe_{17}N_3$ from the nitrogen poor α phase ($Sm_2Fe_{17}N_x \rightarrow Sm_2Fe_{17}N_3$). If the nitrogen dissociation process is the rate determining step for the nitrogenation process, then the profile of homogeneous N atom distribution would be realized just as in Fig. 7(a). This is in contrast to the experimental results. If the nitrogen absorption process is mainly due to the diffusion of nitrogen atoms without the phase transformation of $Sm_2Fe_{17}N_x (x<3.0)$ to $Sm_2Fe_{17}N_3$, the density profile of N atoms shown in Fig. 7(b) would be obtained by the following calculation.

On the assumption that nitrogen content c_N varies only along a certain direction denoted r, the nitrogen atom distribution $c_N(r,t)$ is obtained by the equation of diffusion

$$\frac{\partial c_N}{\partial t}=D\nabla^2 c_N, \tag{2}$$

which is subject to the boundary condition $c_N(0,t)=c_0=3.0$ on the powder surface. Then, the solution of Eq. (2) is given by the following error function:[48]

$$c_N(r,t)=c_0\frac{2}{\sqrt{\pi}}\int_{r/2(Dt)^{1/2}}^{\infty}\exp(-u^2)du. \tag{3}$$

In the calculation, $(Dt)^{1/2}$ is assumed to be much smaller than the powder size. Here, $c_N(r,t)$ is the nitrogen content at the depth r from surface of powder at the reacting time t, and D is the diffusion constant of N atoms in $Sm_2Fe_{17}N_x$, which is normally expressed by the hopping-type model as follows:

$$D=D_0\exp(-Q/kT). \tag{4}$$

Here, D_0 is the preexponential factor, and Q is the activation energy for the hopping process. The values $D_0=1.02\times10^{-6}\,m^2/s$ and $Q=133\,kJ/mol$ were given by Coey *et al.*[40] and Skomski and Coey,[41] respectively.

In this work, it was found that the nitrogen absorption rate was independent of N_2-gas pressures for $P_{N2}\leqq0.05\,MPa$, indicating that the diffusion of N atoms is dominant under lower N_2-gas pressures than 0.05 MPa and determines the reaction rate. Hence, using Eq. (3), we can calculate the nitrogen atom distribution $c_N(r,t)$ at the nitrogenation time t as a function of the depth r, and deduce the resultant nitrogen content $c_N(t)$ at the nitrogenation time t in the powder with a radius r_s using the following equation:

$$c_N(t)=\int_0^{r_S}4\pi r^2 c(r_s-r,t)dr/(4/3)\pi r_s^3. \tag{5}$$

The calculated curve of nitrogen content assuming the diffusion constant $D=3.1\times10^{-16}\,m^2\,s^{-1}$ at 733 K is shown in Fig. 8(a) by the solid line. This curve explains the experimental points obtained for $P_{N2}=0.05\,MPa$. The D value used here is in good agreement with an estimated value of $D=3.3\times10^{-16}\,m^2\,s^{-1}$ from Eq. (4) using $D_0=1.02\times10^{-6}\,m^2\,s^{-1}$ and $Q=133\,kJ\,mol^{-1}$ obtained by Coey and coworkers.[40,41] With increasing the N_2-gas pressure P_{N2}, the

concentration distribution of N atoms could not be understood by only the diffusion process of nitrogen atoms.

When the grain growth of the fully nitrogenated phase $Sm_2Fe_{17}N_3$ becomes dominant in the nitrogenation process, the distribution of N atoms in the powder would be a profile shown in Fig. 7(c). The experimental results shown in Fig. 6 are similar to the model distribution in Fig. 7(c). Then, $c_N(r,t)$ is expressed by the following equation:

$$c_N(r,t)=c_0 \quad \text{for } r \leqslant V_G(P,T)t,$$

$$c_N(r,t)=c_0\frac{2}{\sqrt{\pi}}\int_{r/2(Dt)^{1/2}}^{\infty}\exp(-u^2)du \quad \text{for } r \geqslant V_G(P,T)t. \tag{6}$$

Here, V_G is the velocity of the grain growth of the fully nitrogenated β-phase $Sm_2Fe_{17}N_3$, which increases with increasing N_2-gas pressures. This model quite well explains the experimental results for the nitrogen absorption process under $P_{N2} \geqq 0.1$ MPa. That is, we deduced $V_G = 4.5 \times 10^{-11}\,\mathrm{m\,s^{-1}}$ at 733 K under $P_{N2}=0.1$ MPa from Fig. 6(a) using the relation of $r_t = V_G t$. The nitrogen content $c_N(r,t)$ under $P_{N2}=0.1$ MPa was calculated by substituting $D = 3.1 \times 10^{-16}\,\mathrm{m^2\,s^{-1}}$ and $V_G = 4.5 \times 10^{-11}\,\mathrm{m\,s^{-1}}$ at 733 K obtained independently in Eq. (6). Then, the resultant nitrogen content $c_N(t)$ under $P_{N2}=0.1$ MPa was deduced using Eq. (5), which is drawn by the solid line in Fig. 8(b). Furthermore, the resultant concentration $c_N(r)$ in the gas–solid reaction process at 733 K under 6 MPa was also deduced from Eq. (5) using $c_N(r,t)$ which was calculated by substituting $D = 3.1 \times 10^{-16}\,\mathrm{m^2\,s^{-1}}$ and $V_G = 9.0 \times 10^{-11}\,\mathrm{m\,s^{-1}}$ (estimated from $r_t = V_G t$) into Eq. (6). The calculated result is similarly drawn in Fig. 8(c) by the solid line. The agreement between the calculated and experimental data is quite good for all the cases. Thus, we could clarify the nitrogen absorption process under various N_2-gas pressures in Sm_2Fe_{17}.

Coey *et al.*[40] have claimed that the attractive interatomic long-range interaction energy arising from lattice deformation around the interstitial site is important, and below T_{cri}, the attractive interaction dominates and the interstitial atoms form macroscopic clusters, leading to a two-phase mixture. Above T_{cri}, a solid solution phase should be formed. They estimated T_{cri} for Sm_2Fe_{17} to be about room temperature. On the contrary, Colucci *et al.*[43–45] have inferred that from a metallography study of the nitrogenation process in Nd_2Fe_{17}, the fully nitrided phase directly precipitated from the phase free of nitrogen with no formation of a nitrogen solid-solution phase. The results obtained in this work indicate that the interfacelike propagation model is only acceptable for $P_{N2} \geqq 0.1$ MPa. That is, the diffusion of nitrogen atoms controls the reaction time for nitrogenation at the earlier stage of the nitrogen absorption process, but the grain growth of the fully nitrogenated phase becomes dominant at the later stage of the process under $P_{N2} \geqq 0.1$ MPa. However, under $P_{N2} \leqq 0.05$ MPa, it is very difficult to distinguish which model is acceptable at the late stage of the nitrogenation process because of the random distribution of the activation centers, some local defects, dislocations and so on, playing a relatively important role on the nucleation and growth process. In any case, it seems that the formation of some defects or dislocations accompanied by formation of the N-poor α phase is essential for the grain growth of fully nitrogenated β phase under high N_2-gas pressure.

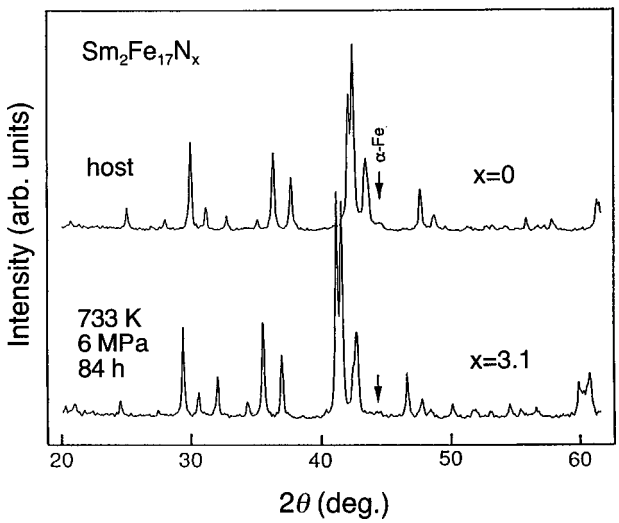

FIG. 9. Powder x-ray-diffraction patterns at room temperature of Sm_2Fe_{17} and $Sm_2Fe_{17}N_{3.1}$ fully nitrogenated at 733 K for 84 h using Cu $K\alpha$ radiation.

Thus, we could deduce that it is useful to apply high-pressure N_2-gas method for obtaining high-quality $R_2Fe_{17}N_3$ powder. According to the above consideration, we can estimate the reaction time for obtaining fully nitrogenated $Sm_2Fe_{17}N_3$ powder with the particle size of $\sim 42 \pm 10\,\mu$m in diameter at 733 K under 6 MPa. The time is deduced to be 84 h from the relation of $r_t = V_G t$ using $2r_t = 42\,\mu$m and $V_G = 9.0 \times 10^{-11}\,\mathrm{m\,s^{-1}}$. The x-ray-diffraction profiles of Sm_2Fe_{17} and $Sm_2Fe_{17}N_{3.3}$ thus produced are shown in Fig. 9. All the diffraction lines shift to lower angles with no line broadening by nitrogenation. No extra peaks are observed in them except for the rhombohedral main peaks. Thus, the above result guarantees the formation of a high-quality nitride with no α-Fe segregation by high-pressure nitrogenation.

V. EFFECT OF NITROGENATION ON MAGNETISM IN $R_2Fe_{17}N_3$ AND $Y_2Co_{17}N_3$

In this section, we present the experimental results on magnetic properties of interstitially modified nitrides $R_2T_{17}N_3$ with R = Y, Ce or Sm and T = Fe or Co, which were done to clarify the influence of N introduction on the overall magnetism.[18] The reasons why we chose Y, Ce, and Sm as the rare earths in this work are as follows: (1) Since Y is nonmagnetic, magnetic studies of this systems are suitable for clarifying magnetism of only the $3d$ sublattice in the 2:17 systems. (2) Since Ce is in an unstable $4f$ state, we can expect a dramatic change in the $4f$-$3d$ hybridization effects by nitrogenation in Ce_2Fe_{17}. (3) As Sm is in a stable trivalent state and has a large second-order Steven's factor, we can easily detect the enhancement of the crystal electric field (CEF) effect due to interstitial modification of nitrogen in Sm_2Fe_{17} from measurements of magnetic anisotropy.

Figure 10 shows the x-ray-diffraction profiles of (a) Y_2Fe_{17} and (b) $Y_2Fe_{17}N_{3.1}$ at room temperature using Cu $K\alpha$ radiation. As is evident from these profiles, both Y_2Fe_{17} and $Y_2Fe_{17}N_{3.1}$ are almost a single phase of the rhombohedral

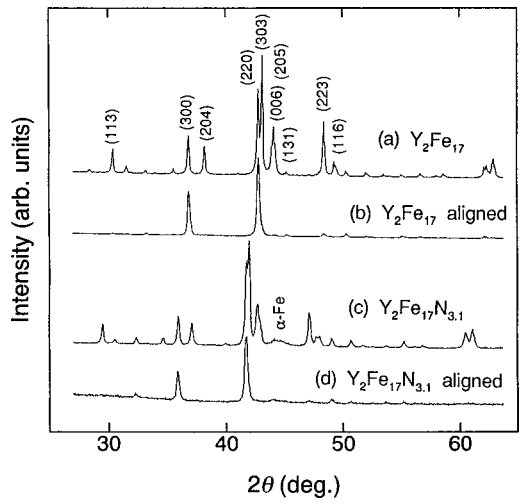

FIG. 10. X-ray-diffraction patterns of Y_2Fe_{17} and $Y_2Fe_{17}N_{3.1}$ at room temperature using Cu $K\alpha$ radiation. Here, (a) and (c) are for the nonaligned powder. (b) and (c) are for the aligned powder along the direction parallel to the x-ray-scattering vector at room temperature.

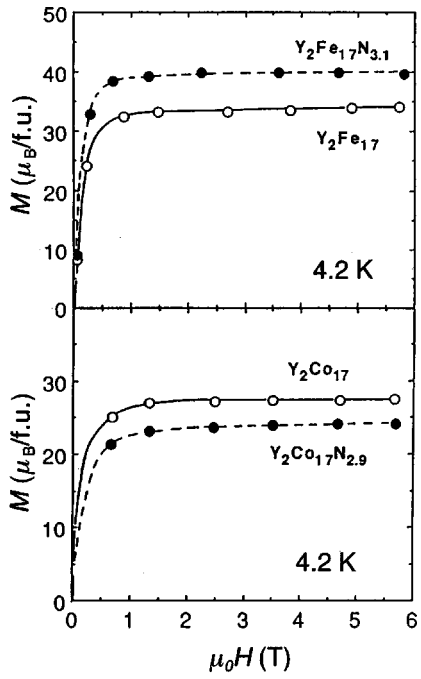

FIG. 11. Magnetization at 4.2 K as a function of magnetic field for Y_2Fe_{17} and Y_2Co_{17} and their nitrides.

Th_2Zn_{17}-type structure except for segregation of a small amount of α-Fe phase in the nitride. All the peaks shift to lower angle by nitrogen absorption, indicating an increase in lattice constants without changing the crystal structure form. In order to check the easy axis of magnetization (EAM), the x-ray-diffraction profiles were examined for magnetically aligned powder along the direction parallel to the scattering vector, the results of which are shown in Figs. 10(b) and 10(d). The enhancement of the (300) and (220) peak intensities indicate that the EAM of both Y_2Fe_{17} and $Y_2Fe_{17}N_{3.1}$ is in the *ab* plane, and the magnetic anisotropy in the Fe sublattice favors the *ab* plane as the direction of magnetization vector even after nitrogenation. The estimated lattice parameters are summarized in Table I, together with those for the other nitrides. Here, we notice that the Y and Sm systems occupy N atoms up to ~3.0 per formula unit and the unit-cell volume homogeneously expands by ~6% upon nitrogenation, while the Ce system occupy N atoms of ~3.6 at interstitial sites and the volume expands by ~9%. The excess nitrogen atoms over 3.0 may occupy the 18*g* interstitial sites after full occupation of the 9*e* interstitial sites, which may lead to the excess volume expansion.[34–36] This can be also speculated from the existence of the excess occupation of the 18*g* sites in addition to full occupation of the 9*e* sites of hydrogen atoms in Ce_2Fe_{17}.[49–51] This large expansion of the unit-cell volume probably induces a conversion of Ce^{4+} into Ce^{3+} due to a drastic decrease in the $4f$-$3d$ hybridization effects as well.[6,52–56]

TABLE I. Structural data of intermetallic compounds R_2Fe_{17} and their nitrides.

Compounds	a (Å)	c (Å)	V (Å^3)	$\Delta a/a_0$ (%)	$\Delta c/c_0$ (%)	$\Delta V/V_0$ (%)
Y_2Fe_{17}	8.51	12.38	776			
$Y_2Fe_{17}N_{3.1}$	8.67	12.69	826	1.9	2.5	6.4
Ce_2Fe_{17}	8.48	12.41	773			
$Ce_2Fe_{17}N_{3.6}$	8.73	12.81	845	2.9	3.2	9.4
Nd_2Fe_{17}	8.58	12.49	796			
$Nd_2Fe_{17}N_3$	8.78	12.67	846	2.3	1.4	6.5
Sm_2Fe_{17}	8.55	12.43	787			
$Sm_2Fe_{17}N_{3.1}$	8.74	12.65	837	2.2	1.8	6.4
Y_2Co_{17}	8.36	12.18	737			
$Y_2Co_{17}N_{2.9}$	8.52	12.45	783	1.9	2.2	6.2

The results of magnetic measurement are summarized in Figs. 11–13 and Table II. As shown in Fig. 11, the saturation moment M_s of $Y_2Fe_{17}N_x$ increases from $34.0\mu_B$ at $x=0$ to $39.7\mu_B$ at $x=3.1$, whereas M_s of $Y_2Co_{17}N_x$ decreases from $27.7\mu_B$ at $x=0$ to $24.1\mu_B$ at $x=2.9$. Similarly, the Curie temperature T_C increases from 300 K at $x=0$ to 701 K at $x=3.1$ for $Y_2Fe_{17}N_X$, while T_C decreases from 1179 K at $x=0$ to 783 K at $x=2.9$ for $Y_2Co_{17}N_X$. Since Y is a nonmagnetic rare-earth element, the change of M_s upon nitrogenation must originate from change of the average $3d$-sublattice moment, which could be explained on the basis of the calculated electronic band structures.[31,57–59] The band calculations simply suggest that the general feature of band structure changes from a weak ferromagnetic to a strong ferromagnetic type in R_2Fe_{17} upon nitrogen uptake,[31,57–59] while it does not change dramatically in R_2Co_{17} upon nitrogenation because of being in a strong ferromagnetic state before nitrogenation.[60] This briefly explains the change of magnetic properties upon nitrogenation. The details will be discussed in the last section.

Another interesting feature in the basic magnetism is that T_C significantly increases for Y_2Fe_{17} upon nitrogen uptake, while T_C significantly decreases for Y_2Co_{17} upon N uptake. According to the spin-fluctuation theory,[61] the general trends of the Curie temperature, the strength of the coupling between the $3d$ magnetic moments on each atomic site can be also described using the electronic band-structure calculations. Then, the Curie temperature T_C is expressed by

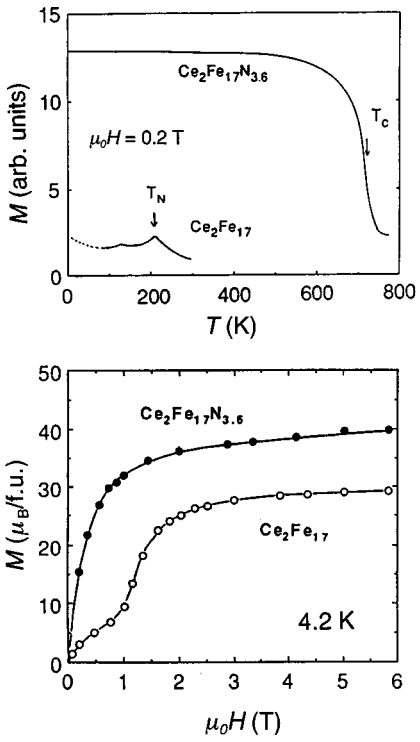

FIG. 12. Magnetization at $\mu_0 H = 0.2$ T vs temperature curves (top) and magnetization at 4.2 K vs field curves (bottom) for Ce_2Fe_{17} and its nitride.

$$T_C \propto M_0^2/\chi_0, \tag{7}$$

where M_0 is the magnetic moment per atom at 0 K and χ_0 is the enhanced susceptibility given by

$$\chi_0^{-1} = \frac{1}{2\mu_B^2}\left(\frac{1}{2N_\uparrow(E_F)} + \frac{1}{2N_\downarrow(E_F)} - I\right). \tag{8}$$

Here, $N_\uparrow(E_F)$ and $N_\downarrow(E_F)$ are the density of states at the Fermi surface E_F for spin-up and spin-down states and I is the Stoner parameter. Jaswal *et al.*[31,57] estimated the increase in T_C upon nitrogen uptake for the Th_2Ni_{17}-type hexagonal Y_2Fe_{17} on the basis of the results of their band calculations, leading to the ratio $T_C(Y_2Fe_{17}N_3)/T_C(Y_2Fe_{17}) = 2.34$. This suggests that an increase in M_0 and a substantial decrease of

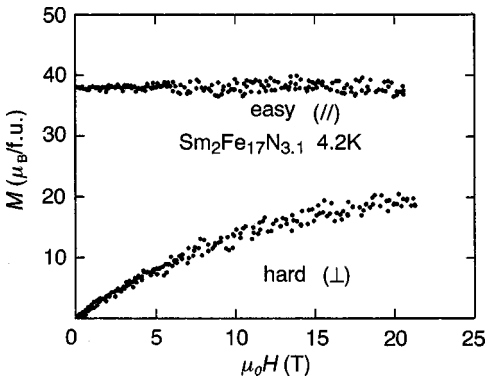

FIG. 13. High-field magnetization as a function of magnetic field for $Sm_2Fe_{17}N_{3.1}$ at 4.2 K along the directions parallel (∥) and perpendicular (⊥) to the aligned direction.

$N_\uparrow(E_F)$ and $N_\downarrow(E_F)$ upon N uptake are essential for almost doubling T_C, and the spin fluctuation is strongly suppressed by interstitial modification of nitrogen. Our experimental results indicate that the situation is almost the same as in the Th_2Zn_{17}-type rhombohedral $Y_2Fe_{17}N_3$. On the other hand, the decrease in T_c for Y_2Co_{17} upon nitrogenation might be originated in the reduction of M_0 in Eq. (7). Therefore, it seems likely that the spin-fluctuation theory is a suitable model for understanding the basic magnetism of rare-earth and $3d$-transition intermetallics at finite temperatures.

Ce_2Fe_{17} is known to show a modified helix with a superstructural magnetic cell along the c axis in the ground state, which changes to a normal helix at $T_t = 110$ K with increasing temperature and finally becomes a paramagnetic state above $T_N = 210$ K.[18,62–64] For understanding these unusual magnetic properties which are different from the other 2:17 Fe compounds, Ce in this system has been considered to be in a tetravalent state.[52–56] In other words, the $4f$ electrons behave as itinerant electrons with a heavy mass owing to the hybridization between the Ce $4f$- and Fe $3d$-electron states.[52–56] As is shown in Fig. 12, nitrogen absorption leads to strong enhancement of ferromagnetism suggesting the conversion of the $4f$ electron from itinerant to localized states. The saturation moment also increases from $29.3\mu_B$ before nitriding to $39.9\mu_B$ after nitriding. A similar conversion is also observed in the case of hydrogen absorption.[49,52,54] Therefore, the conversion might be origi-

TABLE II. Summary of the magnetic data for intermetallic compounds R_2Fe_{17} and their nitrides.

Compounds	M_s (μ_B/f.u.) (4.2K)	T_c (K)	K_1 (kJ/kg) (4.2 K)	K_2 (kJ/kg) (4.2 K)	A_2^0 (Ka_0^{-2}) (4.2 K)	$\mu_0 H_{ex}$ (T)
Y_2Fe_{17}	34.0	300				
$Y_2Fe_{17}N_{3.1}$	39.8	701				
Ce_2Fe_{17}	29.3	210[a]				
$Ce_2Fe_{17}N_{3.6}$	39.9	712				
Nd_2Fe_{17}	39.6	348				
$Nd_2Fe_{17}N_3$	45.3	726				
Sm_2Fe_{17}	34.1	389				
$Sm_2Fe_{17}N_{3.1}$	38.1	752	2.5	2.3	660	510
Y_2Co_{17}	27.7	1179				(~340 K)
$Y_2Co_{17}N_{2.9}$	24.1	783				

[a]Corresponding to Néel temperature.

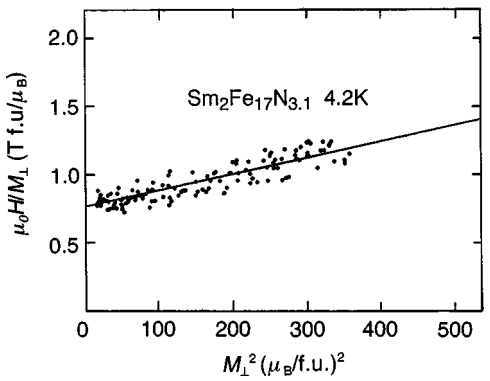

FIG. 14. Sucksumith-Thompson plot for $Sm_2Fe_{17}N_{3.1}$ at 4.2 K; $H/M_\perp$ as a function of $M_\perp^2$.

nated in the decrease in the hybridization of $4f$-$3d$ electron states by lattice expansion accompanied with the interstitial modification.

Using a high-quality nitride $Sm_2Fe_{17}N_{3.1}$ prepared in Sec. III, we measured high-field magnetization at 4.2 K up to 23 T to deduce the reliable magnetic anisotropy constants.[19] The results obtained are shown in Fig. 13. We notice that a strong uniaxial anisotropy in magnetization of aligned powder is induced by nitrogen absorption. Broadly speaking, there are two approaches to understand these extremely anisotropic behaviors; (1) a phenomenological linear model and (2) numerical calculations based on the complete Hamiltonian containing J mixing and noncollinear CEF effects. Since $Sm_2Fe_{17}N_{3.1}$ used in this experiment is an aligned powder but not a single crystal, it is not meaningful to deduce the reliable CEF parameters on the basis of the rigorous calculations. Later, we will describe the numerical and rigorous calculations made for analyzing the magnetization of single-crystalline $Nd_2Fe_{17}N_3$ and obtaining reliable CEF parameters. Here, we apply the phenomenological linear model without any assumption and know how large the enhancement of the apparent magnetic anisotropy in Sm_2Fe_{17} is induced upon nitrogenation.

For a uniaxial crystal, the corresponding uniaxial anisotropy is phenomenologically expressed by

$$E_a = K_1 \sin^2\theta + K_2 \sin^4\theta, \tag{9}$$

where K_1 and K_2 are the apparent uniaxial anisotropy constants, and θ is the angle between the c axis and the resultant magnetization direction. From the minimum condition of the free energy containing the anisotropy energy and Zeeman energy in the linear model, we obtain the following equation without any approximation:[65]

$$\frac{H}{M_\perp} = \frac{2K_1}{M_S^2} + \frac{4K_2}{M_S^4} M_\perp^2. \tag{10}$$

Here, $M_\perp$ is the resultant magnetization along the hard axis at the magnetic field H, and M_S the saturation magnetization. In Fig. 14, we plot $H/M_\perp$ as a function of $M_\perp^2$ for $Sm_2Fe_{17}N_{3.1}$ at 4.2 K. From the straight line, we obtain $K_1 = 2.5\times10^3$ J/kg and $K_2 = 2.3\times10^3$ J/kg. The uniaxial anisotropy constants in $Sm_2Fe_{17}N_3$ have been determined by many authors.[66–69] It is noteworthy that the values obtained in this work are the largest among those reported previously. This might be due to the fact that we used high-quality nitride with almost no host and no α-Fe phases. The appearance of giant uniaxial anisotropy at 4.2 K might be originated in the strong enhancement of the second-order CEF parameter A_2^0 in $R_2Fe_{17}N_3$ upon nitrogen uptake.[68,70] According to Kuz'min and Coey,[68] if we restrict ourselves to the case of zero temperature and neglect the J-mixing effects, K_1 and K_2 are expressed in the first-order approximation as follows:

$$K_1 = -\frac{3}{2}\alpha_J A_2^0 \langle r^2\rangle J(2J-1) - \frac{9}{2}\Delta_{ex}^{-1}(\alpha_J A_2^0\langle r^2\rangle)^2 J(2J-1)^2, \tag{11}$$

$$K_2 = \frac{9}{8}\Delta_{ex}^{-1}(\alpha_J A_2^0\langle r^2\rangle)^2 J(2J-1)(8J-5), \tag{12}$$

where α_J is the second-order Steven factor,[71] A_2^0 is the leading term of the CEF parameters when we express the CEF Hamiltonian as follows:[72]

$$H_{CEF} = \alpha_J A_2^0 \langle r^2\rangle O_s^0(J), \tag{13}$$

where $\langle r^2\rangle$ is the mean of the second power of the $4f$ radius, O_2^0 is the second-order Stevens equivalent operators, and Δ_{ex} is the exchange splitting, which is defined as follows:[68]

$$\Delta_{ex} \equiv |g_J - 1|\mu_B H_{ex}. \tag{14}$$

Here, g_J is the Lande's g factor, H_{ex} is the exchange field acting on rare-earth ions from the Fe sublattice. It is to be noted that those formulas are deduced by considering only the leading term in the CEF interactions and the exchange field acting on rare-earth ions from the Fe sublattice. As an attempt, from the apparent K_1 and K_2 obtained here, we estimated the CEF parameter $A_2^0 = -660\,\mathrm{K}/a_0^2$ and the exchange field $\mu_0 H_{ex} = 510$ T, which corresponds to 340 K, respectively. The theoretical estimations of A_2^0 have been performed from the calculation of electron density distribution for some $R_2Fe_{17}N_3$ so far.[59,73–75] The calculated values of A_2^0 well agree with the experimental one in this work (see Table III). The details of the enhancement of CEF parameters will be discussed in the next section.

VI. INFLUENCE OF NITROGENATION ON CRYSTAL ELECTRIC FIELD AT RARE EARTH IONS IN 2:17 SYSTEM

Since the discovery of the nitride $Sm_2Fe_{17}N_3$, the experimental and theoretical studies of interstitially modified R_2Fe_{17} compounds have been done by many researchers to clarify the drastic improvement in magnetic properties upon nitrogenation.[6] However, their experimental works have been only performed using powder or polycrystalline samples. Especially, for clarifying the effect of nitrogenation

TABLE III. Summary of the CEF analysis for Nd_2Fe_{17} and $Nd_2Fe_{17}N_3$ single crystals at 4.2 K. The data of K_{Fe} for Nd_2Fe_{17} and for $Nd_2Fe_{17}N_3$ were deduced from the results of Refs. 83, 84, and 69. The calculated second-order CEF parameter A_2^0 taken from Refs. 75, 59, and 74 is also listed for comparison of our experimental and calculated values.

	Crystal-field coefficients						$m_{Fe}(\mu_B)$	K_{Fe} (K)	H_{ex} (K)
Compounds	$A_2^0(Ka_0^{-2})$	$A_4^0(Ka_0^{-4})$	$A_4^3(Ka_0^{-4})$	$A_6^0(Ka_0^{-6})$	$A_6^3(Ka_0^{-6})$	$A_6^6(Ka_0^{-6})$			
Nd_2Fe_{17}	-5.0×10^2	-18	2.6	-6.0	-13	1.2×10^2	2.0	-3.4[a,b]	290
$Nd_2Fe_{17}N_3$	-1.5×10^2	-17	-5.5	5.6	7.9	-7.7	2.3	-2.6[c]	360
Sm_2Fe_{17}	-107[d]								
$Sm_2Fe_{17}N_3$	-665[d]								
Gd_2Fe_{17}	-191[e]								
$Gd_2Fe_{17}N_3$	-664[e]								
Gd_2Fe_{17}	-286[f]								
$Gd_2Fe_{17}N_3$	-948[f]								

[a]Reference 83.
[b]Reference 84.
[c]Reference 69.
[d]Reference 75.
[e]Reference 59.
[f]Reference 74.

on CEF parameters in R_2Fe_{17}, it is important to measure the magnetic anisotropy using the single crystal of the interstitial nitride $R_2Fe_{17}N_x$. In this work, we carefully synthesized a $Nd_2Fe_{17}N_3$ single crystal by means of prehydrogenation and the high-pressure N_2-gas nitrogenation technique, starting from single crystals of Nd_2Fe_{17} and carried out the high-field magnetization measurements of both the Nd_2Fe_{17} and $Nd_2Fe_{17}N_3$ single crystals at 4.2 K.

The single crystals of Nd_2Fe_{17} were prepared by a flux method as described in Sec. III. We know that it is essential to avoid the surface contamination for homogeneous and faster nitrogenation in a nitrogen gas–solid reaction process.[14] Hence, we applied the hydrogen decrepitation treatment[76] before nitriding, by which many new clean surfaces were caused. That is to say, the small cubed Nd_2Fe_{17} single crystal was preheated at 573 K in the sample chamber under H_2 gas pressure of 1 MPa for 3 h, and subsequently held in vacuum for 3 h. After then, nitrogenation was performed by heating the single crystal at 723 K for 20 days under a N_2 gas pressure of 6 MPa.[21] After nitrogenation, we confirmed that the cubed Nd_2Fe_{17} single crystal fractured into some granule crystals. Fortunately, the granule with the largest mass obtained was about 2.1 mg in this process. The nitrogen concentration in the single-crystalline nitride was estimated to be ~3 per formula unit from the increase in the mass. This largest single crystal was used for high-field magnetic measurement.

Figure 15 shows the x-ray diffraction (XRD) patterns of (a) Nd_2Fe_{17} and (b) $Nd_2Fe_{17}N_3$ at room temperature using Cu $K\alpha$ radiation, which was examined using the powder sample obtained by grinding some of the granule single crystals. As is evident from this figure, the nitride $Nd_2Fe_{17}N_3$ is confirmed to be almost a single phase except for a very small trace of α-Fe phase. However, no peaks of Nd_2Fe_{17} are observed in the nitride, indicating that the single crystal was fully nitrogenated. The XRD peaks of nitride shifts to lower angles, indicating that the lattice expands without changing the rhombohedral structure upon nitrogenation. The estimated lattice parameters of the nitride are also summarized in Table I. The relative increase in unit-cell volume, $\Delta V/V$, of the nitride $Nd_2Fe_{17}N_3$ is 6.3%, which is in good agreement with the result of neutron power diffraction for $Nd_2Fe_{17}N_{2.9}$ determined by Kajitani *et al.*[36] They have reported that the refined occupation of the N atoms on the 9*e* and the 18*g* sites were 0.95(4) and 0.01(2) in $Nd_2Fe_{17}N_{2.9}$, respectively. In addition, the result of our neutron experiment for the rhombohedral $Y_2Fe_{17}N_{3.1}$ ($\Delta V/V=6.5\%$), which will be described later, have shown that the N atoms fully occupy the 9*e* sites. Therefore, we conclude that the N atoms in the $Nd_2Fe_{17}N_3$ single crystal also fully occupy the 9*e* sites.

In order to check the morphology and the nitrogen distribution in the $Nd_2Fe_{17}N_3$ single crystal, we observed the SEM and EPMA image profiles at the cross section of the Nd_2Fe_{17} and $Nd_2Fe_{17}N_3$ single crystals. The single crystals were polished by a buffing machine using alumina powder with particle size less than 0.05 μm. Figures 16(a) and 16(b) show the EPMA-line profiles and corresponding SEM figures for the Nd_2Fe_{17} and $Nd_2Fe_{17}N_3$ single crystals, respectively. As is seen in Fig. 16(a), the EPMA profile indicates that the Fe and Nd elements homogeneously distribute in the Nd_2Fe_{17} single crystal. On the other hand, as we can see from Fig.

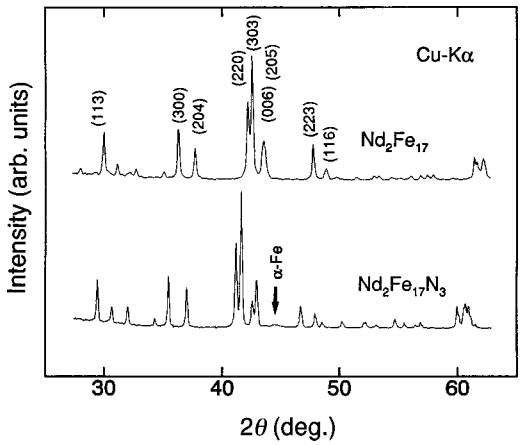

FIG. 15. X-ray powder-diffraction patterns of Nd_2Fe_{17} and $Nd_2Fe_{17}N_3$ (obtained by grinding some of the single crystals) at room temperature using Cu $K\alpha$ radiation.

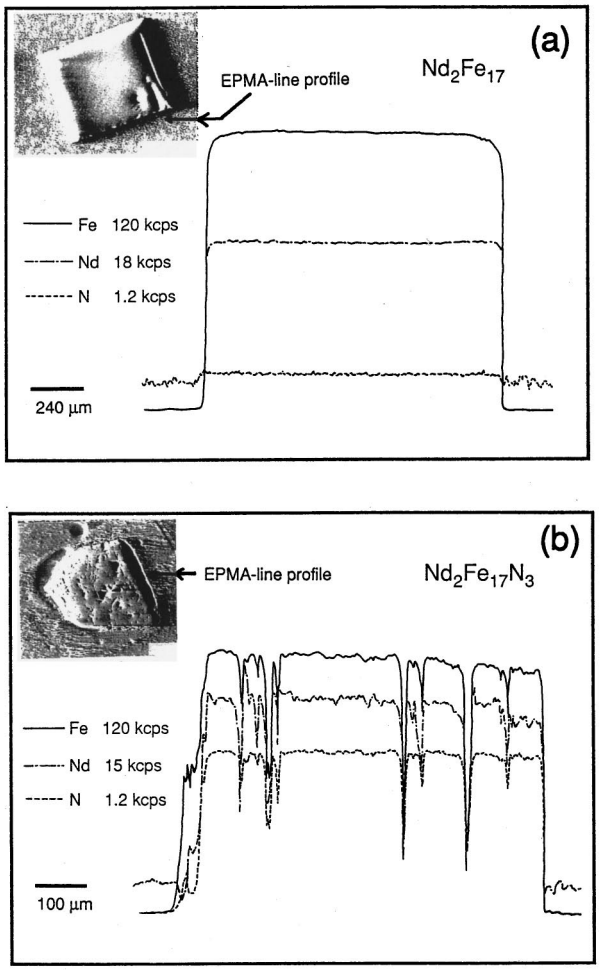

FIG. 16. EPMA line profiles of Nd, Fe, and N elements in the (a) Nd_2Fe_{17} and (b) $Nd_2Fe_{17}N_3$ single crystals. The insets show the corresponding SEM figure.

16(b), it shows that the nitrogen atoms almost homogeneously distribute inside of the $Nd_2Fe_{17}N_3$ single crystal, although there are some microcracks in the single crystal of nitride.

Figure 17 shows the temperature dependence of magnetization, M-T curve, measured in magnetic field of 1 T along the easy b axis for the Nd_2Fe_{17} and $Nd_2Fe_{17}N_3$ single crystals. In this figure, the Curie temperature T_C was determined

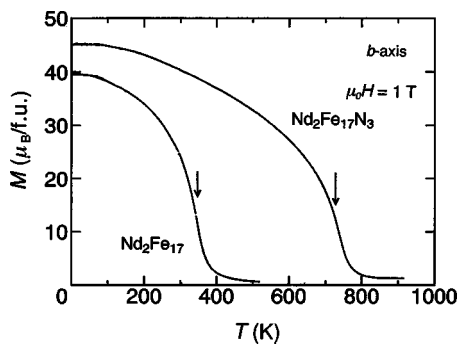

FIG. 17. Temperature dependence of the magnetization along the b axis for the Nd_2Fe_{17} and $Nd_2Fe_{17}N_3$ single crystals. The arrows indicate the temperature corresponding to the Curie temperature.

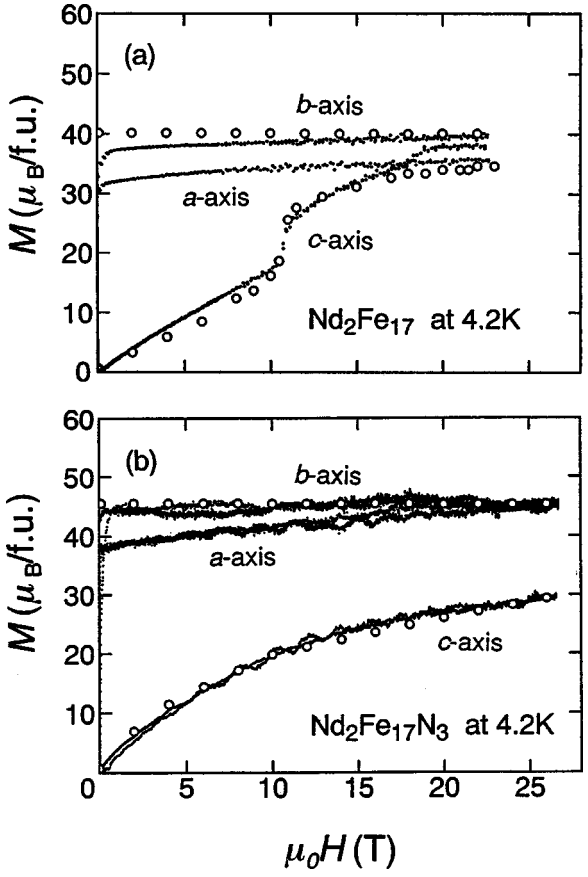

FIG. 18. High-field magnetization curves along the three principal axes for the (a) Nd_2Fe_{17} and (b) $Nd_2Fe_{17}N_3$ single crystals at 4.2 K. Open circles show the calculated magnetization.

as the inflection point of a low-field thermomagnetic curve at $\mu_0H=0.05$ T, the value of which is listed in the Table II. The Curie temperature increases from 348 to 726 K upon nitrogenation. As discussed in Sec. V, we consider that the increase in T_C is due to the suppression of the spin fluctuation mainly caused by the decrease in the density of states of the spin-up and spin-down bands at the Fermi level upon nitrogenation. The M-T curve also shows that $Nd_2Fe_{17}N_3$ is almost single phased except for a small α-Fe phase, the trace of which continues above 900 K. We estimated that the content of the α-Fe phase in the $Nd_2Fe_{17}N_3$ single crystal was $\sim$3% from the value of the magnetization at 900 K in Fig. 17. Thus, all the complementary results of the XRD patterns, the SEM-EPMA analysis and the M-T curves confirmed that the single crystal of the high-quality $Nd_2Fe_{17}N_3$ nitride was successfully synthesized by high-pressure N_2-gas nitrogenation method in this work.

Figure 18 shows the high-field magnetization curves of the (a) Nd_2Fe_{17} and (b) $Nd_2Fe_{17}N_3$ single crystals at 4.2 K. As is seen in Fig. 18, the easy axis of magnetization EAM of Nd_2Fe_{17} is the b axis, the direction of which does not change upon nitrogenation. The saturation magnetic moment M_S was determined from the extrapolation of the M vs $1/H^2$ curve along the b axis to infinite field. The saturation magnetic moment M_S of Nd_2Fe_{17} at 4.2 K increases from 39.6 to 45.3 μ_B/f.u. upon nitrogenation. This increase in M_S upon nitrogenation mainly originates from an increase in the average Fe magnetic moment owing to a decrease in the Fe-Fe

overlap induced by the large lattice expansion ($\Delta V/V \sim 6\%$) as shown in the Secs. V and VII. Furthermore, we recognize that two-step anomalous magnetization jumps for Nd_2Fe_{17} appear around 10 and 18 T in the magnetization curve along the hard *c* axis, which is interpreted as the first-order magnetization process (FOMP).[77] Koide *et al.* have also reported a similar anomalous magnetization process for the $Nd_2(Fe_{0.96}Al_{0.04})_{17}$ single crystal.[78] On the other hand, no magnetization jump along the *c* axis was observed for the nitride $Nd_2Fe_{17}N_3$ in magnetic fields up to 27 T. Generally speaking, a phenomenological description of FOMP in terms of the anisotropy constants K_i or the anisotropy coefficients κ_n^m indicates that the first-order magnetization transition requires the existence of the higher-order terms in the expansion of the free energy.[77] Therefore, the result of no observation of FOMP for $Nd_2Fe_{17}N_3$ may show that the second-order term is strongly enhanced and dominates the anisotropy energy in R_2Fe_{17} upon nitrogenation. On the other hand, it is of interest that the strong anisotropy within the *c* plane is reduced upon nitrogenation.

To clarify the influence of the interstitial N atom introduction on the crystalline electric field (CEF) at the *R* site in R_2Fe_{17} compounds, we analyzed the above magnetization curves on the basis of the rigorous Hamiltonian combined the molecular field and CEF theories in a two-sublattice model,[79] and estimated the CEF parameters A_n^m at the rare-earth site in the 2:17 system.

In the two-sublattice model, the free energy of the system is given by

$$F(\mathbf{H},\theta) = -2k_BT\ln Z + 17K_{\mathrm{Fe}}\sin 2\theta - 17\mathbf{m}_{\mathrm{Fe}}\cdot\mathbf{H}, \quad (15)$$

where k_B, K_{Fe}, $\mathbf{m}_{\mathrm{Fe}}$, and $\mathbf{H}$ are, respectively, the Boltzmann constant, the uniaxial magnetocrystalline anisotropy constant per Fe atom of the Fe sublattice, the Fe magnetic moment and the applied field, and θ is the angle between $\mathbf{m}_{\mathrm{Fe}}$ and the *c* axis. The partition function *Z* is calculated from the eigenvalues of Hamiltonian H_{Nd} for the Nd sublattice. Then, H_{Nd} is represented in a single-ion model by

$$H_{\mathrm{Nd}} = H_{\mathrm{CEF}} + 2(g_J - 1)\mathbf{J}\cdot\mathbf{H}_{\mathrm{ex}} + g_J\mathbf{J}\cdot\mathbf{H}, \quad (16)$$

where H_{CEF} is the CEF Hamiltonian, g_J is the Lande *g* factor, $\mathbf{J}$ is the total angular momentum of Nd, and $\mathbf{H}_{\mathrm{ex}}$ is the exchange field from the Fe sublattice through the Nd-Fe exchange interaction, respectively.

Since the point symmetry of the Nd site ($6c$ site) in the rhombohedral Th_2Zn_{17}-type structure is D_{3d}, the CEF Hamiltonian H_{CEF} for the ground $\mathbf{J}$ multiplet state is expressed by[80]

$$H_{\mathrm{CEF}} = B_2^0O_2^0 + B_4^0O_4^0 + B_4^3O_4^3 + B_6^0O_6^0 + B_6^3O_6^3 + B_6^6O_6^6. \quad (17)$$

Here the parameters O_n^m are the Stevens equivalent operators and B_n^m are written by

$$B_n^m = \theta_n\langle r^n\rangle A_n^m, \quad (18)$$

where A_n^m are the crystal-field parameters, θ_n are the Steven factors $\alpha_J, \beta_J, \gamma_J$, for $n=2$, 4 and 6, respectively, and $\langle r^n\rangle$ is the mean of the *n*th power of the $4f$ radius.[71,72] The values of θ_n, and $\langle r^n\rangle$ have been calculated by Freeman and Watson[81] for R^{3+} ions based on the Hartree-Fock approximation.

The exchange field H_{ex} in Eq. (16) is given by

$$H_{\mathrm{ex}} = -n_{\mathrm{NdFe}}\cdot 17m_{\mathrm{Fe}}/V, \quad (19)$$

where n_{NdFe}, and *V* are the molecular field coefficient between Nd and Fe sublattices, and the unit-cell volume, respectively. The molecular field coefficient n_{NdFe} was estimated from the Curie temperature T_C based on a molecular field model.[82] The estimated value of n_{NdFe} was 3.64×10^{-4} H/m($290\mu_B$).[38] Moreover, as the magnetocrystalline anisotropy constant K_{Fe}, we used the data of a hexagonal Y_2Fe_{17} single crystal[83,84] or the data of a hexagonal $Y_2Fe_{17}N_3$ powder aligned in a rotating magnetic field,[69] assuming that the anisotropy constant in the rhombohedral Y_2Fe_{17} or $Y_2Fe_{17}N_3$ has the same value as in the hexagonal ones. The used values of m_{Fe}, K_{Fe}, and H_{ex} in this analysis are summarized in Table III. Under the condition of making the free energy $F(\mathbf{H},\theta)$ minimum, the CEF parameters A_n^m were determined by a least-squares fitting so as to minimize $\Delta = \Sigma(M_{\mathrm{exp}} - M_{\mathrm{cal}})^2$, where M_{exp} and M_{cal} are the experimental and calculated magnetic moments, respectively.

The final values of parameters estimated are summarized in Table III. It is to be noted that the A_n^m values estimated for Nd_2Fe_{17} are in good agreement with the values deduced by considering the excited $\mathbf{J}$ multiplet for a $Nd_2(Fe_{0.96}Al_{0.04})_{17}$ single crystal reported by Koide *et al.*[78] The open circles in Fig. 18 show the calculated magnetization using the estimated A_n^m values. The agreement between the experimental curve and calculated magnetization one deduced by the numerical analysis is quite good, and the anomalous magnetization jumps are also reproduced around 10 and 18 T for Nd_2Fe_{17}. We notice that the sign of A_2^0 does not change by nitrogen uptake, but the magnitude of $A_2^0(=-15\times10^2\ \mathrm{K}/a_0^2)$ for the $Nd_2Fe_{17}N_3$ is strongly enhanced by about three times as large as that of $A_2^0(=-5.0\times10^2\ \mathrm{K}/a_0^2)$ for Nd_2Fe_{17}.

On the basis of our experimental results, we discuss the origin of the enhancement of the magnetocrystalline anisotropy of R_2Fe_{17} due to nitrogen uptake. From the CEF analysis for magnetization curves of the Nd_2Fe_{17} single crystal, we have estimated that A_2^0 at the rare-earth (*R*) site in R_2Fe_{17} is $-5.0\times10^2\ \mathrm{K}/a_0^2$ at 4.2 K. This suggests that the EAM of the Sm sublattice in Sm_2Fe_{17} is the *c* axis, i.e., the uniaxial anisotropy constant of the *R* sublattice, $K_1^R>0$ from the relation of $K_1^R = -(3/2)N_R\alpha_J\langle r^2\rangle 2J(J-1)A_2^0$ driven by Lindgard and Danielsen,[70] because the sign of α_J for Sm is positive. However, the EAM of Sm_2Fe_{17} is in the basal *ab* plane at room temperature, indicating that at room temperature the basal plane anisotropy of the Fe sublattice probably overcomes the easy *c*-axis anisotropy of the Sm sublattice in Sm_2Fe_{17}. Since the magnitude of negative A_2^0 is strongly enhanced upon nitrogenation, the uniaxial anisotropy of $Sm_2Fe_{17}N_3$ is dominated by the easy *c*-axis anisotropy of the Sm sublattice even at room temperature but not the plane anisotropy from the Fe sublattice.

Coehoorn has proposed a simple model based on Miedema's ''macroscopic atom'' idea,[85,86] from which the

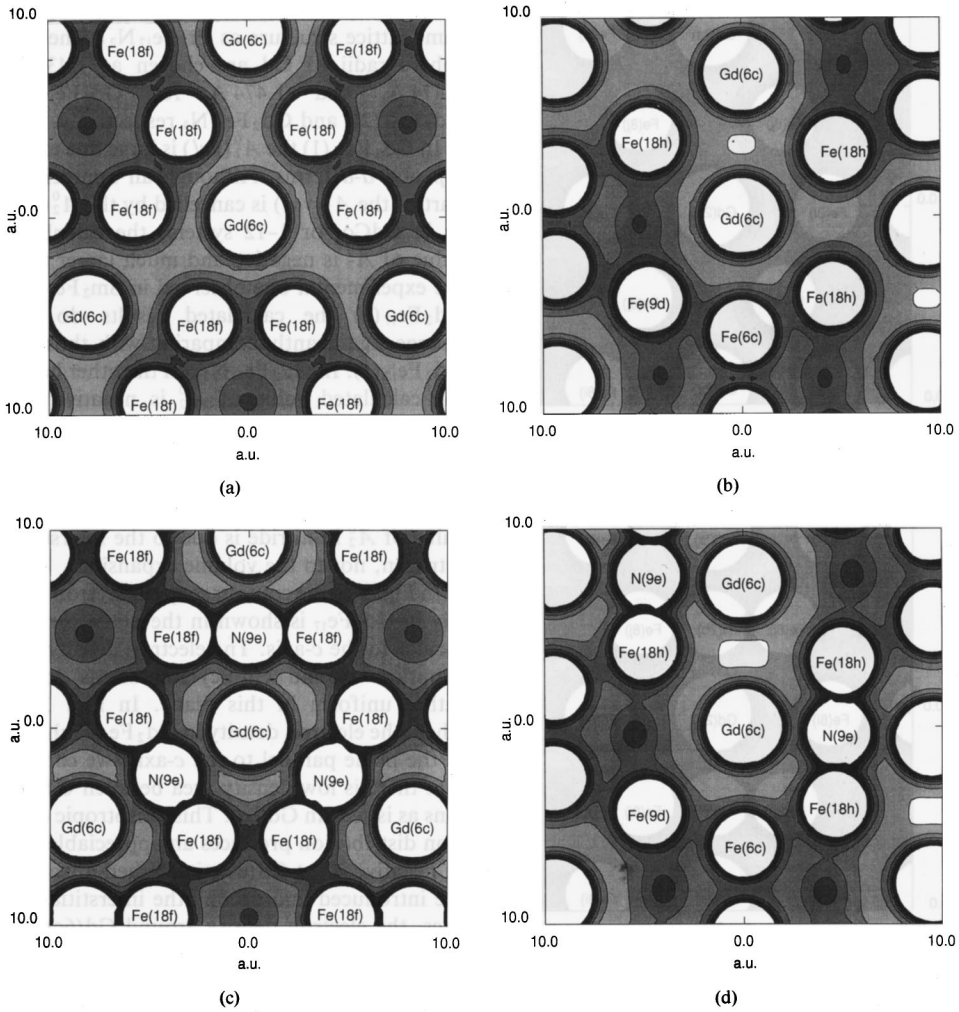

FIG. 19. Electron density distribution of Gd_2Fe_{17}; (a) in a plane perpendicular to the c axis and (b) in a plane parallel to the c axis, and $Gd_2Fe_{17}N_3$; (c) in a plane perpendicular to the c axis and (d) in a plane parallel to the c axis. The lowest contour value is 0.0125 a.u.$^{-3}$, the contour spacing is 0.0125 a.u.$^{-3}$, and the highest contour value is 0.1 a.u.$^{-3}$. The lowest density regions in (b) and (d) have densities between 0 and 0.0125 a.u.$^{-3}$. The density regions with those higher than 0.1 a.u.$^{-3}$ near each atomic site are not shaded. These are calculated using a full-potential APW method by Yamaguchi and Asano (Ref. 74).

trends in the second-order CEF coefficient and the magnetocrystalline anisotropy could be understood qualitatively.[87] According to this simple model, the charge density at the boundary of the Wigner-Seitz cell, the Miedema parameter n_{WS} (Refs. 85, 86) acts as an important factor, and the following qualitative prediction for A_2^0 on a certain rare-earth site can be satisfied: (1) If the position of its neighbors with the highest values of n_{WS} is within or close to the plane perpendicular to the c axis containing the rare-earth atom, Δn_p and Δn_d are expected to be positive ($A_2^0<0$). (2) On the other hand, Δn_p and Δn_d are expected to be negative if these neighbors are situated on or close to the line parallel to the c axis through the central rare-earth atom ($A_2^0>0$). Here, the parameters Δn_p and Δn_d, which give the degree to which the p and d shells are prolate or oblate, are defined in terms of the occupation numbers as follows:

$$\Delta n_p=(n_x+n_y)/2-n_z, \tag{20}$$

and

$$\Delta n_d=n_{x^2-y^2}+n_{xy}-(n_{xz}+n_{yz})/2-n_{z^2}, \tag{21}$$

where n_x, n_y, and n_z are the occupation numbers of the p_x, p_y, p_z orbitals and $n_{x^2-y^2}$, n_{xy}, n_{xz}, n_{yz} and n_{z^2} are occupation numbers of the d_{x2-y2}, d_{xy}, d_{zx}, d_{yz} and d_{z2} orbitals, respectively. That is to say, assuming that A_2^0 is mainly originated from the asphericity of the rare-earth valence electron charge density, the relation between A_2^0 and Δn_l $(l=p,d)$ can be expressed from Coehoorn's model[85,88,89] as follows:

$$A_2^0 \propto -\Delta n_l. \tag{22}$$

From our experimental results for the Nd_2Fe_{17} and $Nd_2Fe_{17}N_3$ single crystals, we found that A_2^0 estimated for Nd_2Fe_{17} was negative and the magnitude increased about three times by nitrogenation. This result indicates that Δn_l is positive and remarkably increases upon nitrogenation. The value of electronegativity of the N atoms is larger than that of the R atoms. In addition, the value of n_{WS} of the N atoms ($\sim$4) is larger than that of the R atoms ($\sim$2).[85,86] Therefore, when nitrogen atoms are introduced and occupy the interstitial $9e$ sites, the high charge density of the rare-earth valence

(p and d) electrons may be formed at the cell boundary between the R ion at the $6c$ site and the N ion at the $9e$ site within the basal ab plane. This valence electron configuration is probably an origin of the large enhancement of negative A_2^0 upon nitrogenation, leading to the strong uniaxial anisotropy of $Sm_2Fe_{17}N_3$.

On the other hand, calculations of electronic charge density have been carried out by Yamaguchi and Asano[59,74] for Gd_2Fe_{17} and $Gd_2Fe_{17}N_3$ and by Steinbeck *et al.*[75] for Sm_2Fe_{17} and $Sm_2Fe_{17}N_3$ to understand the origin of large enhancement of negative A_2^0 upon nitrogenation. According to Yamaguchi and Asano's calculations, the electron density distribution around the Gd($6c$) ions seems to be rather uniform in the ab plane, while in the plane parallel to the c axis, there is a low density area between the Gd($6c$) ions [see Figs. 19(a) and 19(b)]. This anisotropic electron distribution produces an appreciably negative A_2^0 at the Gd site. When nitrogen atoms are introduced and occupy the interstitial $9e$ sites, the electron density around the Gd($6c$) ions changes as follows [See Figs. 19(c) and 19(d)]. That is to say, the N $2p$ electrons strongly hybridize with $5d$ electrons of the Gd($6c$) atoms in the ab plane, leading to an increase in the electron density around the Gd($6c$) ions in the ab plane. As a result of such an additional anisotropy of the electron density distribution upon nitriding, A_2^0 at the Gd($6c$) site in $R_2Fe_{17}N_3$ is about ~ 3 times larger than that in Gd_2Fe_{17}. These deduced values for A_2^0 from the calculation of charge distributions are also given in Table III. The calculated values of A_2^0 upon nitrogenation qualitatively agree with our experimental data, which was directly evaluated from the magnetization curves of the single crystal. However, it should be noted that the magnitude of A_2^0 for $Nd_2Fe_{17}N_3$ is almost twice larger than calculated one for $Sm_2Fe_{17}N_3$ and $Gd_2Fe_{17}N_3$. Further studies are necessary from the theoretical points of view.

VII. EFFECT OF NITROGENATION ON Fe MOMENT AT EACH DIFFERENT ATOMIC SITE IN Y_2Fe_{17}

As mentioned in Sec. IV, the introduction of nitrogen atoms into the R_2Fe_{17} compounds led to remarkable increases in T_C and magnetic moments of the Fe-sublattice accompanied by a large increase in unit-cell volume ($\sim 6\%$) without changing the crystal structure. For clarifying the role that the interstitial N atoms played on the microscopic scale for magnetism, it is necessary to know the change of the Fe magnetic moment on each different site upon nitrogenation. The neutron-diffraction experiments, which are the most direct method to microscopically elucidate both the crystallographic and magnetic properties, have been carried out by a number of research groups on some R_2Fe_{17} nitrides so far.[12,28–37,90] In those experiments, it has been clarified that the N atoms mainly occupied the $9e$ site in the rhombohedral 2:17 structure and led to the increase in the average Fe moment, but detailed information on the change of the Fe moment at each atomic site due to nitrogen uptake has not been obtained yet except for a few reports[12,36] as far as we know.

To elucidate in detail the magnetism of the Fe sublattice in the $R_2Fe_{17}N_3$ system, we studied the high-resolution neutron powder-diffraction study on the rhombohedral Y_2Fe_{17} and $Y_2Fe_{17}N_x$ with no partial disorder.[22] Until now, the experiment using the good quality rhombohedral $Y_2Fe_{17}N_x$ has not been reported yet, because it was too difficult to obtain the single phased sample. The neutron-diffraction patterns of Y_2Fe_{17} and $Y_2Fe_{17}N_{3.1}$ at 10 K are shown by the dotted points in Fig. 20, together with the calculated lines. Prior to the analysis, the intensity data of neutron diffraction for Y_2Fe_{17} and $Y_2Fe_{17}N_{3.1}$ from $2\theta = 10°$ to 153° at 10 K were used in the structure refinements using RIETAN-94,[91,92] which was developed for an application of the Rietveld method.[93] The neutron-scattering lengths used for the refinement were $b_Y = 7.750$, $b_{Fe} = 9.540$, and $b_N = 9.360$ in units of 10^{-15} m. Evaluation of the fit between the observed and calculated patterns could be done by the reliability factors R_p, R_I, and R_F, with

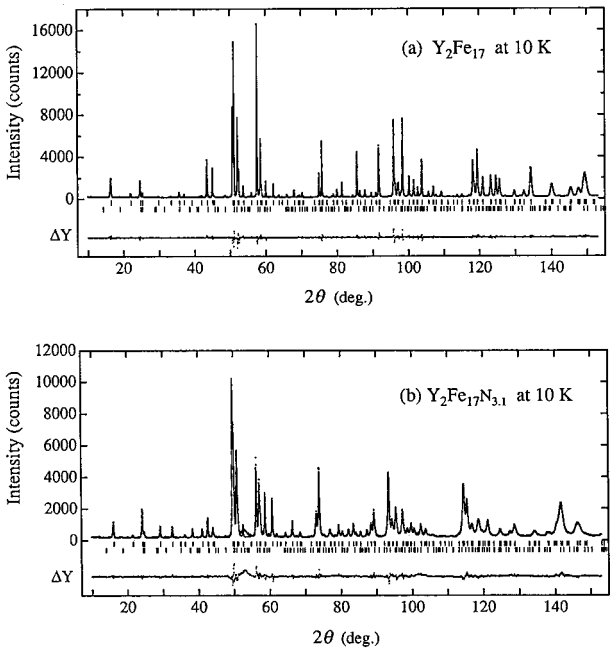

FIG. 20. Neutron powder-diffraction patterns of (a) Y_2Fe_{17} and (b) $Y_2Fe_{17}N_{3.1}$ at 10 K. Here, the dots and lines correspond to the observed and calculated patterns, respectively. The lower part is the difference pattern between the observed and calculated data. The calculated peak positions of the rhombohedral and the hexagonal phases are indicated by the first and second bars, respectively.

$$R_p = \frac{\Sigma |y_i(o) - y_i(c)|}{\Sigma y_i(o)}, \quad R_I = \frac{\Sigma |I_k(o) - I_k(c)|}{\Sigma I_k(o)}, \quad \text{and}$$

$$R_F = \frac{\Sigma |\sqrt{I_k(o)} - \sqrt{I_k(c)}|}{\Sigma \sqrt{I_k(o)}}, \tag{23}$$

where $y_i(o)$ and $y_i(c)$ are the observed and the calculated intensities, respectively, $I_k(o)$ and $I_k(c)$ are the integrated intensities of the observed kth peak and the calculated peak, respectively.

Since the existence of a very weak peak ($2\theta = 48.8°$) corresponding to the (203) reflection for the hexagonal structure was confirmed, the refinements of the diffraction pattern of the host and nitride were performed assuming that the sample contains a small amount of the secondary hexagonal phase in the main rhombohedral phase. For the rhombohedral structure, the lattice parameters used as initial values

TABLE IV. Refined parameters for rhombohedral phase of Y_2Fe_{17} at 10 K. n is the occupation factor; x, y, and z are the fractional coordinate; B is the isotropic thermal parameter (Å^2); and m is the magnetic moment (μ_B/atom). Numbers in parentheses are the statistical error given by the refinement program.

Y_2Fe_{17} 10 K $R_p=5.62\%$							
Rhombohedral $R_I=3.16\%$ $R_F=1.83\%$							
$a=8.5003(1)$ Å $c=12.4294(1)$ Å							
Atom	Site	n	x	y	z	B	m
Y	6c	1.0	0	0	0.3413(6)	0.61(2)	0
Fe(1)	6c	1.0	0	0	0.0960(4)	0.310(1)	2.23(5)
Fe(2)	9d	1.0	0.5	0	0.5	0.310	1.88(6)
Fe(3)	18f	1.0	0.2954(3)	0	0	0.310	1.94(2)
Fe(4)	18h	1.0	0.1672	−0.1672(2)	0.4910(2)	0.310	1.87(4)

were those obtained by XRD studies at room temperature, and the coordinates of atoms were taken from the results for Nd_2Fe_{17} reported by Kajitani *et al.*[36] For the hexagonal structure, the starting structural model without partial disorder was set on the basis of the hexagonal Y_2Fe_{17} reported by Yelon *et al.*[34] In respect to the refinement of the magnetic moments, we adopted an analytical approximation to the magnetic form factor for Fe.[94] In addition, we assumed that both the Y and N moments are $0\mu_B$, and the Fe moments are collinear within the *ab* plane. The initial values of the Fe magnetic moments on all the sites were taken as the average moment obtained by magnetization measurement. In this case, the Fe moment at each site in the hexagonal structure was constrained to be the same value as that at each equivalent site in the rhombohedral structure. Parameters were refined in the following order; (1) background, scale, and profile parameters, (2) structural parameters of the rhombohedral phase, (3) structural parameters of the hexagonal phase, and finally, (4) all parameters including magnetic moments and isotropic-thermal parameters. The obtained structural data are summarized in Table IV. As is seen in Fig. 20(a), the calculated patterns for Y_2Fe_{17} are in very good agreement with the observed patterns. From the results of the refinements, we found that the hexagonal phase is contaminated ~4% in the sample as a secondary phase.

For the nitride $Y_2Fe_{17}N_{3.1}$, a small and broad peak corresponding to α-Fe segregation upon nitrogenation appears around $2\theta=53.4°$. It was difficult to get a good overall profile fitting because of a too broad peak of the α-Fe phase. Therefore, the refinements for the nitride were performed except for the data points in the 2θ range from 52.5 to 54.5°. Among the previous neutron-diffraction data for $R_2Fe_{17}N_x$, there have been some reports that N atoms only occupy the 9e interstitial sites,[12,28–30,32,33,37,90] or that a small amount of N atoms also occupy the 18g interstitial sites in addition to the 9e sites.[31,34–36] Then, we carried out the refinements assuming the following two different models: (1) the N atoms occupy only the 9e interstitial sites in the rhombohedral structure (one-site model); and (2) the N atoms occupy both the 9e and the 18g interstitial sites (two-site model). In both models, the refined occupation of the N atoms in the 6h and 12i interstitial sites in the hexagonal structure was constrained to be the same as that on the corresponding to the 9e and 18g sites in the rhombohedral structure, respectively. Adopting the one-site model for the nitride at 10 K, the R factors reached $R_p=6.53$, $R_I=3.42$, and $R_F=2.31\%$, and the refined occupation of the N atoms became 1.004(7). On the other hand, the R factors for the two-site model at 10 K were deduced to be $R_p=6.12$, $R_I=2.96$, and $R_F=1.97\%$, and the refined occupation of the N atoms on the 9e and the 18g interstitial sites were 0.995(5) and 0.039(2), respectively. These R factors are so close between the above two models that we cannot decide which model is better in this case. So, we analyzed here the data, independently, for the above two models. The refined structure data are summarized in Tables V (one-site model) and VI (two-site model). As is evident from these tables, the crystallographic parameters fitted by both the models are almost the same values except for the Fe magnetic moments. The lattice parameters

TABLE V. Refined parameters for rhombohedral phase of $Y_2Fe_{17}N_{3.1}$ at 10 K, assuming that the N atoms occupy only the 9e site. Symbols have the same meaning and units as in Table IV.

$Y_2Fe_{17}N_{3.1}$ 10 K $R_p=6.53\%$							
Rhombohedral $R_I=3.42\%$ $R_F=2.31\%$							
$a=8.6710(3)$ Å $c=12.7240(4)$ Å							
Atom	Site	n	x	y	z	B	m
Y	6c	1.0	0	0	0.338(1)	0.79(4)	0
Fe(1)	6c	1.0	0	0	0.0947(6)	0.225(6)	2.38(6)
Fe(2)	9d	1.0	0.5	0	0.5	0.225	2.19(9)
Fe(3)	18f	1.0	0.2829(5)	0	0	0.225	2.16(3)
Fe(4)	18h	1.0	0.1705(3)	−0.1705	0.4860(4)	0.225	2.43(6)
N(1)	9e	1.003(7)	0.5	0	0	0.66(6)	0

TABLE VI. Refined parameters for rhombohedral phase of $Y_2Fe_{17}N_{3.1}$ at 10 K, assuming that the N atoms occupy both the 9*e* and the 18*g* sites. Symbols have the same meaning and units as in Table IV.

$Y_2Fe_{17}N_{3.1}$ 10K $R_p=6.21\%$							
Rhombohedral $R_I=2.97\%$ $R_F=1.97\%$							
$a=8.6710(3)$ Å $c=12.7241(4)$ Å							
Atom	Site	*n*	*x*	*y*	*z*	*B*	*m*
Y	6*c*	1.0	0	0	0.338(1)	0.85(4)	0
Fe(1)	6*c*	1.0	0	0	0.0949(6)	0.202(7)	2.86(5)
Fe(2)	9*d*	1.0	0.5	0	0.5	0.202	2.12(8)
Fe(3)	18*f*	1.0	0.2829(5)	0	0	0.202	2.01(4)
Fe(4)	18*h*	1.0	0.1703(3)	−0.1703	0.4860(4)	0.202	2.41(5)
N(1)	9*e*	0.995(5)	0.5	0	0	0.65(5)	0
N(2)	18*g*	0.039(2)	0.08(1)	0	0.5	0.65	0

a and *c* at 10 K increase by 2.0 and 2.4%, respectively, upon nitrogenation. The nitrogen contents deduced from the occupation factors are 3.0 for one-site model and 3.2 for two-site model, respectively. These nitrogen contents are also comparable with the value 3.1 ± 0.1 estimated from the increase in sample mass. From the above structure refinements, we can conclude that the N atoms fully occupy the 9*e* site. In addition, it is possible that a small amount of the N atoms also occupy the 18*g* site in the nitride synthesized by high-pressure nitrogen absorption process.

The deduced Fe magnetic moments on crystallographically different sites in Y_2Fe_{17} and $Y_2Fe_{17}N_{3.1}$ at 10 K are summarized in Table VII, together with the data obtained by magnetization measurements at 4.2 K. We notice that the total magnetic moments m_T for Y_2Fe_{17} increases by 17% upon nitrogen absorption for both the two models and are in good agreement with the values obtained by magnetization measurements. As is evident from Table VII, the site-dependent Fe moments for the host and nitride are observed. For Y_2Fe_{17} at 10 K, the Fe atom at the 6*c* site has the largest moment, whereas the Fe atoms at the 9*d* and the 18*h* sites have the smallest moments. Although the value of the Fe moment at each different site in the nitride is different from each other in the above two models, we notice a common tendency for the site dependence to be $m(6c)\geqslant m(18h)>m(9d)\geqslant m(18f)$ in the nitride. That is to say, the Fe magnetic moments at all the nonequivalent sites increase upon nitrogenation, but the Fe moment at the 18*f* site in $Y_2Fe_{17}N_{3.1}$ is the lowest.

Both the interatomic and average Fe-Fe distances for the rhombohedral host compound and nitride at 10 K are listed in Tables VIII and IX, respectively. On the basis of the Fe-Fe and Fe-N bond distances, the difference of the Fe magnetic moments in nonequivalent Fe sites in the host compound and nitride is qualitatively understood as follows. For Y_2Fe_{17}, the highest Fe moment of $2.23\mu_B$ at the 6*c* site is probably due to the smallest overlap between 3*d*-electron wave functions of iron atoms, because the average Fe-Fe distance between Fe atoms at the 6*c* site and the other near-neighboring sites is the largest relative to the others. On the contrary, the small values of the Fe moments in the 9*d* and the 18*h* sites (1.88 and $1.87\mu_B$) in Y_2Fe_{17} are probably due to a relatively large overlap of 3*d* electron wave functions owing to shorter near-neighboring Fe-Fe distances on average. Here it is noteworthy that the magnitude of the Fe moments does not correlate with the nearest-neighboring Fe-Y distances. This may be

TABLE VII. Magnetic moments of different atomic sites and total moment per formula unit m_T in Y_2Fe_{17} and $Y_2Fe_{17}N_{3.1}$ at 10 K for both the one-site and two-site models. The calculated data are also taken from Refs. 95, 64 and 59.

		$m_{Fe}(\mu_B)$						
Compound rhombohedral	$m_Y(\mu_B)$ 6*c*	6*c*	9*d*	18*f*	18*h*	$m_N(\mu_B)$ 9*e*	$m_T(\mu_B$/f.u.)	Method
Y_2Fe_{17} (expt)	0	2.23(5)	1.88(6)	1.94(2)	1.87(4)		33.0	Neutron, 10 K
Y_2Fe_{17} (expt)							33.6	Magnetization, 4.2 K
Y_2Fe_{17} (calc)	−0.29	2.29	1.91	2.25	1.97		35.1	scASW,[a] 0 K
Y_2Fe_{17} (calc)	−0.63	2.52	2.05	2.37	2.10		36.8	scOLCAO,[b] 0 K
Y_2Fe_{17} (calc)	−0.34	2.53	1.51	2.10	1.98		33.4	LMTO-ASA,[c] 0 K
$Y_2Fe_{17}N_{3.1}$ (expt)	0	2.38(6)	2.19(9)	2.16(3)	2.43(6)	0	38.9	Neutron, 10 K (one-site)
$Y_2Fe_{17}N_{3.1}$ (expt)	0	2.86(5)	2.12(8)	2.01(4)	2.41(5)	0	38.6	Neutron, 10 K (two-site)
$Y_2Fe_{17}N_{3.1}$ (expt)							38.7	Magnetization, 4.2 K
$Y_2Fe_{17}N_3$ (calc)	−0.46	2.55	2.50	2.02	2.31	−0.07	37.5	scOLCAO,[b] 0 K
$Y_2Fe_{17}N_3$ (calc)	−0.29	2.66	2.42	1.94	2.30	0.05	37.6	LMTO-ASA,[c] 0 K

[a]Reference 95.
[b]Reference 58.
[c]Reference 59.

TABLE VIII. Interatomic distances (Å) of rhombohedral Y_2Fe_{17} and $Y_2Fe_{17}N_{3.1}$ at 10 K, which is evaluated from Table VI. Symbol p is the multiplicity of each distance.

Bond	p	Y_2Fe_{17}	$Y_2Fe_{17}N_{3.1}$
Y-Fe(3)f	6	3.009(1)	3.132(2)
Y-Fe(1)c	1	3.054(8)	3.09(2)
Y-Fe(4)h	3	3.086(5)	3.16(1)
Y-Fe(4)h	3	3.201(5)	3.180(8)
Y-Fe(4)h	3	3.222(5)	3.40(1)
Y-Fe(2)d	3	3.278(5)	3.315(8)
Y-N(1)e	3		2.5037(3)
Fe(1)c-Fe(1)c	1	2.38(1)	2.41(2)
Fe(1)c-Fe(2)d	3	2.607(2)	2.665(3)
Fe(1)c-Fe(4)h	3	2.639(4)	2.681(6)
Fe(1)c-Fe(3)f	6	2.780(3)	2.734(5)
Fe(1)c-Y	1	3.054(8)	3.09(1)
Fe(1)c-N(1)e	3		3.933(6)
Fe(2)d-Fe(3)f	4	2.4384(4)	2.4790(5)
Fe(2)d-Fe(4)h	4	2.452(2)	2.483(2)
Fe(2)d-Fe(1)c	2	2.607(2)	2.665(3)
Fe(2)d-Y	2	3.278(5)	3.315(8)
Fe(2)d-N(1)e	4		3.2807(1)
Fe(3)f-Fe(2)d	2	2.4384(4)	2.4790(5)
Fe(3)f-Fe(3)f	2	2.511(2)	2.453(4)
Fe(3)f-Fe(4)h	2	2.531(3)	2.626(4)
Fe(3)f-Fe(4)h	2	2.622(3)	2.705(5)
Fe(3)f-Fe(1)c	2	2.780(3)	2.734(5)
Fe(3)f-Y	2	3.009(1)	3.132(3)
Fe(3)f-Fe(3)f	1	3.476(5)	3.764(8)
Fe(3)f-N(1)e	1		1.882(4)
Fe(4)h-Fe(2)d	2	2.452(2)	2.483(2)
Fe(4)h-Fe(4)h	2	2.471(3)	2.583(5)
Fe(4)h-Fe(3)f	2	2.531(3)	2.626(4)
Fe(4)h-Fe(3)f	2	2.622(3)	2.705(4)
Fe(4)h-Fe(1)c	1	2.639(4)	2.681(6)
Fe(4)h-Y	1	3.086(5)	3.16(1)
Fe(4)h-Y	1	3.201(5)	3.180(8)
Fe(4)h-Y	1	3.222(5)	3.40(1)
Fe(4)h-N(1)e	1		1.943(4)
N(1)e-Fe(3)f	2		1.882(4)
N(1)e-Fe(4)h	2		1.943(4)
N(1)e-Y	2		2.5037(3)

due to the fact that the Fe-Y distance is much longer than the Fe-Fe distance on average.

When the N atoms occupy the 9e interstitial sites, the all Fe moments probably increase due to a reduction in the Fe-Fe overlap caused by the increase in the average Fe-Fe distance. However, the enhancement of the magnetic moment of the 18f-Fe atoms upon nitrogenation, which are the nearest to the 9e-N atoms, is the lowest owing to the hybridization between the Fe 3d states and the N 2p states. On the contrary, the 6c-Fe and/or 18h-Fe atoms, which are farther from the 9e-N atoms and from the environmental Fe atoms on average, have the highest magnetic moments because of weakest hybridizations of the 3d electrons on their Fe sites with the environmental Fe 3d-electron states and N 2p-electron states.

TABLE IX. Average Fe-Fe interatomic distances (Å) of rhombohedral Y_2Fe_{17} and $Y_2Fe_{17}N_{3.1}$ at 10 K.

Site	Y_2Fe_{17}	$Y_2Fe_{17}N_{3.1}$
Fe(1)c	2.680	2.680
Fe(2)d	2.478	2.518
Fe(3)f	2.658	2.705
Fe(4)h	2.532	2.608

The calculated Fe moments located at the different sites and the total magnetic moment per formula unit in the rhombohedral form of Y_2Fe_{17} and $Y_2Fe_{17}N_3$ (Refs. 58,59,95) are given in Table VII. There is a substantial correspondence between the experimental and the calculated values at the same Fe sites. Especially, we notice that the agreement for the two-site model is better than that for the one-site model. However, the results obtained by the calculation are in a little disagreement with our experimental data in details. That is, the calculations shows that the moment of 18f-Fe atoms with the N nearest neighbors in the nitride is smaller than that in the host compound. Nevertheless, the experiments indicate that an increase in the 18f-Fe moment slightly increases upon nitrogenation, irrespective of the model. We believe that it is necessary to make a more sophisticated electronic band structure calculation for understanding the change of microscopic magnetism as well as the CEF parameters upon nitrogenation.

VIII. CONCLUSION

In this work, we have systematically studied fundamental physical properties of interstitially modified nitrides $R_2Fe_{17}N_3$ (R=Y, Ce, Nd, and Sm) and $Y_2Co_{17}N_3$. From the SEM-EPMA analysis of nitrogen distribution in $Sm_2Fe_{17}N_3$ which was synthesized under various N_2-gas pressure up to 6 MPa, we clarified that under low N_2-gas pressure, nitrogen absorption into the grain interior is mainly due to diffusion of nitrogen atoms, while under high N_2-gas pressure, nitrogen absorption is promoted by the grain growth of the fully nitrogenated $Sm_2Fe_{17}N_3$ phase rather than diffusion. Furthermore, we found that the high-pressure N_2-gas nitrogenation process is suitable for synthesizing high-quality nitrides.

The magnetization measurements using high-quality host compounds and their nitrides showed that the saturation magnetization and Curie temperature of Y_2Fe_{17} significantly increase upon nitrogenation, whereas the saturation magnetization and Curie temperature of Y_2Co_{17} decrease. To experimentally clarify the influence of the interstitial nitrogen atom on A_2^0 in R_2Fe_{17}, a bulky single crystal of the $R_2Fe_{17}N_3$ nitride has been prepared in present work by means of the high-pressure N_2 gas nitrogenation technique followed by prehydrogenation. The results of high-field magnetization measurements for the Nd_2Fe_{17} and $Nd_2Fe_{17}N_3$ single crystals at 4.2 K indicated that A_2^0 reaches up to -1.5×10^3 K/a_2^0 at 4.2 K upon nitrogenation, which is about three times as large as that for Nd_2Fe_{17}. This indicates that the appearance of the strong uniaxial anisotropy of Sm_2Fe_{17} upon nitrogenation is due to the strong enhancement of A_2^0 upon interstitial modi-

fication of the N atoms near the R atoms in R_2Fe_{17}. On the other hand, we have also performed neutron-diffraction measurements on Y_2Fe_{17} and $Y_2Fe_{17}N_{3.1}$ for obtaining information on the change of the Fe magnetic moment on each site in the Fe sublattice upon nitrogenation. The introduction of N atoms into Y_2Fe_{17} leads to a strong modification of the Fe magnetic moment. The magnetic moment of the 18f-Fe atoms which are the nearest to the 9e-N atoms in $Y_2Fe_{17}N_{3.1}$ is the lowest value, whereas the 6c-Fe and/or 18h-Fe atoms being farther from the 9e-N atoms and the environmental Fe atoms on average have the highest magnetic moments. These results indicate that the difference of the Fe moments on nonequivalent sites strongly correlates with the Fe-Fe and Fe-N bond distances, which qualitatively agrees with the result of electronic band-structure calculation.

ACKNOWLEDGMENTS

We should like to thank our experimental and theoretical collaborators for having been part of this work. In particular, we are very much indebted to Professor T. Kajitani, Professor Y. Morii, Professor M. Motokawa, Professor S. Mitudo, Professor Y. Andoh, Dr. S. Suzuki, K. Tatami, and Professor P. C. Canfield for valuable experimental supports and discussion. This work was supported by an International Joint Research Project of the NEDO, Japan, and a Grant-in-Aid for Scientific Research from the Ministry of Education, Science and Culture, Japan. We would like to thank the staff members of the High field Laboratory of Institute for Materials Research, Tohoku University, and Japan Atomic Energy Research Institute.

*Author to whom correspondence should be addressed: Faculty of Integrated Arts and Sciences, Hiroshima University, 1-7-1 Higashi-Hiroshima 739-8521, Japan. Electronic address: hfujii@ipc.hiroshima-u.ac.jp

[1] G. Wiesinger and G. Hilscher, in *Handbook of Magnetic Materials*, edited by K. H. J. Buschow (Elsevier, Amsterdam, 1991), Vol. 6, p. 511.
[2] X.-Z. Wang, K. Donelly, J. M. D. Coey, B. Chevalier, J. Etourneau, and T. Berlureau, J. Mater. Sci. **23**, 329 (1988).
[3] M. Sagawa, S. Fujimura, H. Yamamoto, Y. Matsuura, and K. Hiraga, IEEE Trans. Magn. **MAG-20**, 1584 (1984).
[4] J. J. Croat, J. F. Herbst, R. W. Lee, and F. E. Pinkerton, J. Appl. Phys. **55**, 2078 (1984).
[5] J. F. Herbst, Rev. Mod. Phys. **63**, 819 (1991).
[6] H. Fujii and H. Sun, in *Handbook of Magnetic Materials*, edited by K. H. J. Buschow (Elsevier, Amsterdam, 1995), Vol. 9, p. 511.
[7] S. Higano, K. Yamagata, K. Tokoro, M. Fukuda, and K. Kamino, IEEE Trans. Magn. **MAG-23**, 3098 (1987).
[8] J. M. D. Coey and H. Sun, J. Magn. Magn. Mater. **87**, L251 (1990).
[9] M. Katter, J. Wecker, L. Schultz, and R. Grössinger, J. Magn. Magn. Mater. **117**, 419 (1992).
[10] T. Iriyama, K. Kobayashi, N. Imaoka, T. Fukuda, H. Kato, and Y. Nakagawa, IEEE Trans. Magn. **Mag-28**, 2326 (1992).
[11] H. H. Uchida, H. Uchida, T. Yanagisawa, S. Kise, V. Koeninger, Y. Matsumura, U. Koike, T. Kurino, and H. Kaneko (unpublished).
[12] O. Isnard, S. Miraglia, J. L. Soubeyroux, and D. Fruchart, J. Alloys Compd. **190**, 129 (1992).
[13] H. Fujii, K. Tatami, M. Akayama, and K. Yamamoto, in *Proceedings of the 6th International Conference on Ferrites*, 1992, Tokyo and Kyoto, Japan (The Japan Society of Powder and Powder Metallurgy, Tokyo, 1992), p. 1081.
[14] H. Fujii, K. Tatami, and K. Koyama, J. Alloys Compd. **236**, 156 (1996).
[15] K. Machida, A. Shiomi, H. Izumi, and G. Adachi, Jpn. J. Appl. Phys., Part 2 **34**, L741 (1995).
[16] A. Kawamoto, T. Ishikawa, S. Yasuda, K. Takeya, K. Ishizuka, T. Iseki, and K. Ohmori, IEEE Trans. Magn. **35**, 3322 (1999).
[17] I. Sasaki, H. Fujii, H. Okada, and S. Suzuki, IEEE Trans. Magn. **35**, 3319 (1999).
[18] H. Fujii, M. Akayama, K. Nakao, and K. Tatami, J. Alloys Compd. **219**, 10 (1995).
[19] H. Fujii, K. Koyama, I. Sasaki, S. Mistudo, and M. Motokawa, J. Magn. Soc. Jpn. **23**, 465 (1999).
[20] K. Koyama, H. Fujii, S. Mitudo, M. Motokawa, J. Kojima, Y. Andoh, and P. C. Canfield, Physica B **237–238**, 548 (1997).
[21] K. Koyama, H. Fujii, S. Mitudo, M. Motokawa, J. Kojima, Y. Andoh, and P. C. Canfield, J. Magn. Soc. Jpn. **22**, 245 (1998), in Japanese.
[22] K. Koyama, T. Kajitani, Y. Morii, H. Fujii, and M. Akayama, Phys. Rev. B **55**, 11 414 (1997).
[23] A. Iandelli and A. Palenzona, in *Handbook on the Physics and Chemistry of Rare Earths*, edited by K. A. Gschneidner, Jr. and L. R. Eyring (Elsevier, Amsterdam, 1979), Vol. 2, p. 1.
[24] K. H. J. Buschow, Phys. Status Solidi A **7**, 199 (1971).
[25] K. H. J. Buschow, Rep. Prog. Phys. **40**, 1179 (1971).
[26] D. Givord, R. Lemaire, J. M. Moreau, and D. Roudaut, J. Less-Common Met. **29**, 361 (1972).
[27] A. Christensen and R. F. Hazell, Acta Chem. Scand. **A34**, 455 (1980).
[28] R. M. Ibberson, O. Mozze, T. H. Jacobs, and K. H. J. Buschow, J. Phys.: Condens. Matter **3**, 1219 (1991).
[29] O. Isnard, S. Miraglia, J. L. Soubeyroux, D. Fruchart, and R. Pannetier, Phys. Rev. B **45**, 2920 (1992).
[30] S. Miraglia, J. L. Soubeyroux, C. Kolbeck, O. Isnard, D. Fruchart, and M. Guillot, J. Less-Common Met. **171**, 51 (1991).
[31] S. S. Jaswal, W. B. Yelon, G. C. Hadjipanayis, Y. Z. Wang, and D. J. Sellmyer, Phys. Rev. Lett. **67**, 644 (1991).
[32] Y. C. Yang, Z. D. Zhang, L. S. Kong, Q. Pan, J. L. Yang, Y. F. Ding, B. S. Zhang, C. T. Ye, and L. Jin, J. Appl. Phys. **70**, 6018 (1991).
[33] O. Isnard, J. L. Soubeyroux, S. Miraglia, D. Fruchart, L. M. Garcia, and J. Bartolome, Physica B **180-181**, 624 (1992).
[34] W. B. Yelon and G. C. Hajipanayis, IEEE Trans. Magn. **MAG-28**, 2316 (1992).
[35] Q. W. Yan, P. L. Zhang, Y. N. Wei, K. Sun, B. P. Hu, Y. Z. Wong, G. C. Liu, C. Gan, and Y. F. Cheng, Phys. Rev. B **48**, 2878 (1993).
[36] T. Kajitani, Y. Morii, S. Funahashi, T. Iriyama, K. Kobayashi, H. Kato, Y. Nakagawa, and K. Hiraga, J. Appl. Phys. **73**, 6032 (1993).
[37] O. Isnard, S. Miraglia, J. L. Soubeyroux, D. Fruchart, J. Deports, and K. H. J. Buschow, J. Phys.: Condens. Matter **5**, 5481 (1993).
[38] K. Koyama, H. Fujii, and P. C. Canfield, Physica B **226**, 363 (1996).

[39] T. Mukai and T. Fujimoto, J. Magn. Magn. Mater. **103**, 165 (1992).
[40] J. M. D. Coey, R. Skomski, and S. Wirth, IEEE Trans. Magn. **Mag-28**, 2332 (1992).
[41] R. Skomski and J. M. D. Coey, J. Appl. Phys. **73**, 7602 (1993).
[42] S. Brennan, R. Skomski, Q. Qi, and J. M. D. Coey, J. Magn. Magn. Mater. **140-144**, 999 (1995).
[43] C. C. Colucci, S. Gama, L. C. Labaki, and F. A. O. Cabral, IEEE Trans. Magn. **28**, 2578 (1992).
[44] C. C. Colucci, S. Gama, L. C. Labaki, and C. A. Ribeiro, J. Alloys Compd. **189**, 45 (1992).
[45] C. C. Colucci, S. Gama, and C. A. Ribeiro, J. Alloys Compd. **194**, 181 (1993).
[46] R. Barrett, D. Fruchart, and J. L. Soubeyroux, J. Alloys Compd. **219**, 193 (1995).
[47] Y. D. Zhang, J. I. Budnick, W. A. Hines, and D. P. Yang, Appl. Phys. Lett. **67**, 208 (1995).
[48] H. Mehrer, N. Stolica, and N. A. Stolwijk, in *Numerical Data and Functional Relationship in Science and Technology*, New Series III, Diffusion in Metals and Alloys, edited by O. Madelung (Springer-Verlag, Berlin, 1990), Vol. 26, p. 32.
[49] O. Isnard, S. Miraglia, J. L. Soubeyroux, D. Fruchart, and A. Stergiou, J. Less-Common Met. **162**, 273 (1990).
[50] O. Isnard, J. L. Soubeyroux, S. Miraglia, D. Fruchart, L. M. Garcia, and J. Bartolome, Physica B **180-181**, 629 (1993).
[51] O. Isnard, S. Miraglia, J. L. Soubeyroux, D. Fruchart, and P. l'Heritier, J. Magn. Magn. Mater. **137**, 151 (1994).
[52] O. Isnard, S. Miraglia, D. Fruchart, and J. Deportes, J. Magn. Magn. Mater. **103**, 157 (1992).
[53] J. M. D. Coey, J. E. M. Allan, A. A. Minakov, and Yu. V. Bugaslarsky, J. Appl. Phys. **73**, 5430 (1993).
[54] O. Isnard, S. Miraglia, D. Fruchart, G. Giorgetti, S. Pizzini, E. Dartyge, G. Krill, and J. P. Kapper, Phys. Rev. B **49**, 15 692 (1994).
[55] H. Sun, J. M. D. Coey, Y. Otani, and D. P. F. Hurley, J. Phys.: Condens. Matter **2**, 6465 (1990).
[56] D. Vandormael, F. Grandijean, V. Briois, D. P. Middleton, K. H. Buschow, and G. J. Long, Phys. Rev. B **56**, 6100 (1997).
[57] S. S. Jaswal, IEEE Trans. Magn. **MAG-28**, 2322 (1992).
[58] W. Y. Ching, M. Z. Huang, and X. F. Zhong, J. Appl. Phys. **76**, 6047 (1994).
[59] S. Asano and M. Yamaguchi, Physica B **237-238**, 541 (1997).
[60] J. Inoue and M. Shimizu, J. Phys. F: Met. Phys. **15**, 1511 (1985).
[61] P. Mohn and E. P. Wohlfarth, J. Phys. F: Met. Phys. **16**, 2421 (1987).
[62] D. Givord and R. Lemaire, IEEE Trans. Magn. **MAG-10**, 109 (1974).
[63] Y. Janssen, H. Fujii, T. Ekino, K. Izawa, T. Suzuki, T. Fujita, and F. R. de Boer, Phys. Rev. B **56**, 13 716 (1997).
[64] H. Fukuda, Y. Janssen, H. Fujii, T. Ekino, and Y. Morii, J. Magn. Soc. Jpn. **23**, 108 (1999).
[65] W. Sucksmith and J. E. Thompson, Proc. R. Soc. London, Ser. A **225**, 362 (1954).
[66] T. S. Zhao, X. C. Kou, R. Grössinger, and H. R. Kirchmayr, Phys. Rev. B **44**, 2846 (1991).
[67] H. Kato, M. Yamada, G. Kido, Y. Nakagawa, T. Iriyama, and K. Kobayashi, J. Appl. Phys. **73**, 6931 (1993).
[68] M. D. Kuz'min and J. M. D. Coey, Phys. Rev. B **50**, 12 533 (1994).
[69] S. Brennan, R. Skomski, D. Cugat, and J. M. D. Coey, J. Magn. Magn. Mater. **140-144**, 971 (1995).
[70] P. A. Lindgard and O. Danielsen, Phys. Rev. B **11**, 351 (1975).
[71] K. W. H. Stevens, Proc. Phys. Soc. London, Sect. A **65**, 209 (1952).
[72] M. T. Hutchings, in *Solid State Physics: Advances in Research and Applications*, edited by F. Seitz and D. Turnbull (Academic, New York, 1964), Vol. 16, p. 227.
[73] R. Coehoorn and G. H. D. Daalderop, J. Magn. Magn. Mater. **104-107**, 1081 (1992).
[74] M. Yamaguchi and S. Asano, J. Phys. Soc. Jpn. **63**, 1071 (1994).
[75] M. Steinbeck, M. Richter, U. Nitzsche, and H. Eschrig, Phys. Rev. B **53**, 7111 (1996).
[76] Sugimoto, Nakamura, Okada, and Homma (Ref. 13), p. 1145.
[77] G. Asti, in *Ferromagnetic Materials*, edited by K. H. J. Buschow and E. P. Wohlfarth (Elsevier, Amsterdam, 1990), Vol. 5, p. 397.
[78] T. Koide, H. Kato, J. Shiomi, T. Iriyama, and M. Yamada, J. Magn. Magn. Mater. **140-144**, 983 (1995).
[79] M. Yamada, H. Kato, H. Yamamoto, and Y. Nakagawa, Phys. Rev. B **38**, 620 (1988).
[80] U. Walter, J. Phys. Chem. Solids **45**, 401 (1984).
[81] A. J. Freeman and R. E. Watson, Phys. Rev. **127**, 2058 (1962).
[82] E. Belorizky, M. A. Fremy, J. P. Gavigan, D. Givord, and H. S. Li, J. Appl. Phys. **61**, 3971 (1987).
[83] S. Sinnema, Ph.D. thesis, University of Amsterdam, 1988.
[84] B. Matthaei, J. J. Franse, S. Sinnema, and R. J. Radwanski, J. Phys. (Paris), Colloq. **49**, C8-533 (1988).
[85] F. R. de Boer, R. Room, W. C. M. Mattens, A. R. Miedema, and A. K. Niessen, in *Cohesion in Metals*, edited by F. R. de Boer and D. G. Pettifor (North-Holland, Amsterdam, 1988).
[86] A. R. Miedema, Physica B **182**, 1 (1992).
[87] R. Coehoorn, J. Magn. Magn. Mater. **99**, 55 (1991).
[88] R. Coehoorn, K. H. J. Buschow, M. W. Dirken, and R. C. Thiel, Phys. Rev. B **42**, 4645 (1990).
[89] R. Coehoorn and K. H. J. Buschow, J. Appl. Phys. **69**, 5590 (1991).
[90] T. Kajitani, Y. Morii, T. Iriyama, and H. Kato, Physica B **213-214**, 294 (1995).
[91] F. Izumi, in *The Rietveld Method*, edited by R. A. Young (Oxford University Press, Oxford, 1993), p. 236.
[92] Y. I. Kim and F. Izumi, J. Ceram. Soc. Jpn. **102**, 401 (1994).
[93] H. M. Rietveld, J. Appl. Crystallogr. **2**, 65 (1969).
[94] P. J. Brown, in *The International Tables for Crystallography*, edited by A. J. C. Wilson (Kluwer, Dordrecht, 1995), Vol. C, p. 391.
[95] R. Coehoorn, Phys. Rev. B **89**, 13 072 (1989).
[96] Y. D. Zhang, J. I. Budnick, D. P. Yang, G. W. Fernand, W. A. Hines, T. D. Xian, and T. Manzur, Phys. Rev. B **51**, 12 091 (1995).
[97] Y. D. Zhang, J. I. Budnick, W. A. Hines, and D. P. Yang, J. Appl. Phys. **79**, 4596 (1996).